Exact asymptotic expansions for the cylindrical Poisson–Boltzmann equation

Gabriel Téllez[1] and Emmanuel Trizac[2,3]

[1] Departamento de Física, Universidad de Los Andes, AA 4976, Bogotá, Colombia
[2] CNRS, Université Paris Sud, UMR 8626, LPTMS, Orsay Cedex, F-91405, France
[3] Center for Theoretical Biological Physics, UC San Diego, 9500 Gilman Drive MC 0374, La Jolla, CA 92093-0374, USA
E-mail: gtellez@uniandes.edu.co and trizac@lptms.u-psud.fr

Abstract. The mathematical theory of integrable Painlevé/Toda type systems sheds new light on the behaviour of solutions to the Poisson–Boltzmann equation for the potential due to a long rod-like macroion. We investigate here the case of symmetric electrolytes together with that of 1:2 and 2:1 salts. Small and large scale features are analysed, with particular emphasis on the low salinity regime. Analytical expansions are derived for several quantities relevant for polyelectrolyte theory, such as the Manning radius. In addition, accurate and practical expressions are worked out for the electrostatic potential, which improve upon previous work and cover the full range of radial distances.

J. Stat. Mech. (2006) P06018

Contents

1. Introduction

Polyelectrolytes are polymer molecules bearing charged units. Within the associated relevant cylindrical geometry, the long range character of Coulombic interactions is responsible for the phenomenon of counterion condensation. In essence, the electric potential created by the charged polyion features a logarithmic dependence on radial distance. The competing entropy of confinement is of a similar functional form, which may result in a condensation of counterions onto the charged cylinder, when Coulombic interactions prevail, that is when the polyelectrolyte line charge exceeds a given threshold (see e.g. [1]). Strongly charged linear polyelectrolytes thereby effectively reduce their line charge density. This was realized by Onsager in the 1960s and formalized subsequently [2,3]. It turns out that the mean field Poisson–Boltzmann (PB) theory

offers a valuable framework for discussing and analysing the phenomenon in detail [4]–[15]. Unfortunately, even within the mean field, exact results are scarce, and one has to resort to numerical resolution or propose approximations.

This paper is dedicated to the derivation of exact results within PB theory. We will be interested in the behaviour of a unique infinite charged cylinder of radius a and uniform line charge density e/b, where $e > 0$ is the elementary charge and b may be viewed as an equivalent average spacing between charges along the polyion. This macroion is immersed in an infinite electrolyte containing two species of microions (salt): their bulk densities n_1 and n_2 far from the cylinder define the Debye length $1/\kappa$ through $\kappa^2 = 4\pi\ell_{\mathrm{B}}(n_1 z_1^2 + n_2 z_2^2)$. Here, $z_i e$ denotes the charge of species i and $\ell_{\mathrm{B}} = \beta e^2/\varepsilon$ is the Bjerrum length, which involves the solvent dielectric permittivity ε and the inverse temperature β. We will focus on the three situations where analytical progress is possible: 1:1 electrolytes (or more generally symmetric z:z electrolytes), together with the 1:2 and 2:1 cases. We denote by 1:2 the situation where coions are monovalent ($z_+ = 1$ for a positively charged polyion) and counterions are divalent ($z_- = -2$ or more generally, $z_- = -2z_+$). On the other hand, the notation 2:1 refers to divalent coions with monovalent counterions. To be specific, introducing the dimensionless radial distance $\tilde{r} = \kappa r$, the equations to be solved for the dimensionless electrostatic potential $y = \beta e \psi$ (ψ being the electric potential) read

$$\frac{\mathrm{d}^2 y}{\mathrm{d}\tilde{r}^2} + \frac{1}{\tilde{r}}\frac{\mathrm{d}y}{\mathrm{d}\tilde{r}} = \sinh(y) \qquad (1:1) \tag{1.1a}$$

$$\frac{\mathrm{d}^2 y}{\mathrm{d}\tilde{r}^2} + \frac{1}{\tilde{r}}\frac{\mathrm{d}y}{\mathrm{d}\tilde{r}} = \frac{1}{3}\left(\mathrm{e}^{2y} - \mathrm{e}^{-y}\right) \qquad (1:2) \tag{1.1b}$$

$$\frac{\mathrm{d}^2 y}{\mathrm{d}\tilde{r}^2} + \frac{1}{\tilde{r}}\frac{\mathrm{d}y}{\mathrm{d}\tilde{r}} = \frac{1}{3}\left(\mathrm{e}^{y} - \mathrm{e}^{-2y}\right) \qquad (2:1). \tag{1.1c}$$

The solution should satisfy the boundary conditions at $\tilde{a} = \kappa a$

$$\lim_{\tilde{r}\to\tilde{a}} \tilde{r}\frac{\mathrm{d}y}{\mathrm{d}\tilde{r}} = -2\,\xi \tag{1.2}$$

and $\lim_{\tilde{r}\to\infty} y(\tilde{r}) = 0$. We have introduced here the dimensionless bare line charge $\xi = \ell_{\mathrm{B}}/b$, that plays a key role below. It is understood that the cylinder is positively charged, without loss of generality[4].

We shall not comment here the well documented limitations of the mean field approximation (see e.g. [16]–[21]), but only summarize the main findings. In a solvent like water at room temperature, mean field provides an accurate description in the 1:1 case for all existing polyelectrolytes. We also expect the 2:1 situation to be correctly described, while in the 1:2 case, microionic correlations, discarded within the mean field, play an important role at large values of ξ. Schematically, the coupling parameter $\Gamma = z^{3/2}\sqrt{\xi\ell_{\mathrm{B}}/(2\pi a)}$ allows one to appreciate the importance of those correlations where z stands for the counterion valency. When $\Gamma < 2$, the mean field holds.

The crux of our approach lies in the mapping between equations (1.1) and Painlevé/Toda type equations (see below), that are in particular relevant for describing the spin–spin correlator in the two-dimensional Ising model, and have been the subject of deep

---

[4] Note that the 1:2 case with $\xi > 0$, with coions of valency $z_1 = +1$ and counterions of valency $z_2 = -2$, is identical to the case $z_1 = +2$, $z_2 = -1$ with $\xi < 0$. Equation (1.1c) and the boundary condition (1.2) is of course formally equivalent to equation (1.1b) after the substitutions $y \to -y$ and $\xi \to -\xi$.

mathematical investigations [22]–[24]. It seems that this body of work has not been fully transposed into the language of polyelectrolyte physics, with the exception of for the limit $\kappa a \to 0^+$ (e.g. realized with a charged line—of vanishing thickness—at finite salt) where it allowed several authors to show rigorously the existence of the condensation [9, 10] and also provided exact results for the electric potential [9, 11]. However, it will appear below that the limit $\kappa a \to 0^+$ is approached logarithmically slowly so that finite salt correction cannot be neglected in practice. It also turns that to the best of our knowledge, the case of 2:1 electrolytes has not been considered in the physics literature, whereas some results have been reported in the reverse 1:2 case, but below the condensation threshold and again in the limit $\tilde{a} \to 0$ [11]. Our aim is to fill these gaps. Our formulae will prove extremely accurate when compared to the numerical solutions of (1.1).

The paper is organized as follows. In section 2, the formal solutions of equations (1.1) will be given. As such, these relations are not useful in practice, and deriving 'ready-to-use' and operational expressions will be the purpose of the subsequent analysis. Section 3 will then be devoted to the derivation of asymptotic expansions for the electric potential, and to the connection between short and long distance features. These results identify a change in the short distance behaviour when increasing the charge density above a threshold $\xi_{\rm c}$, which will be worked out. This is the fingerprint of counterion condensation, which turns out to be smoothed by salt (strictly speaking, the phenomenon is critical in the limit $\kappa a \to 0$ only). Section 4 will analyse a few limiting cases of particular interest. Analytical expressions for several important quantities such as the Manning radius will be given and compared in section 5 to the numerical data obtained solving the non-linear PB equation. A similar analysis will be performed for the electric potential, which will assess the validity of the analytical results. Although particular attention will be paid to the low salinity regime (the results of sections 3–5 rely on expansions that typically break down for $\kappa a > 1$), we will also report in section 6 some results concerning the effective charge of the polyion, valid for all values of κa. A preliminary account of parts of this work has been published in [25].

Before embarking on the analysis of the properties of equations (1.1), we note that for a macroion with a small reduced linear charge density $\xi_{\rm eff}$, the problem may be linearized with the solution

$$y_{\rm lin}(\tilde{r}) = \frac{2\xi_{\rm eff}}{\tilde{a}K_1(\tilde{a})}K_0(\tilde{r}). \tag{1.3}$$

Here K_0 and K_1 are the modified Bessel functions. Since the solution to the non-linear problem (1.1) vanishes when $\tilde{r} \to \infty$ we necessarily have that for large distances $\tilde{r}$, $y(\tilde{r})$ behaves as (1.3). However in the non-linear case the constant $\xi_{\rm eff}$ is not the bare charge of the rod. This quantity is called the effective charge and depends on salinity conditions, bare charge, temperature etc. In the weak overlap approximation where the double layers of different macroions are well separated (it is typically the case when their mutual distance is larger than $1/\kappa$), the (squared) effective charge governs the amplitude of the interaction free energy.

2. Formal solution to the problem

The Poisson–Boltzmann equation (1.1a) in the 1:1 case has been solved in [22] in the context of the Painlevé III theory, since $e^{y/2}$ obeys a particular case of the Painlevé III

equation (see e.g. [26] and appendix A; more details together with a relevant bibliography may be found in [27]). More generally, equations (1.1a), (1.1b) and (1.1c) are the first equations of the hierarchy of cylindrical Toda equations. In [23], a class of solutions to these Toda equations has been reported, and hence the solutions to the Poisson–Boltzmann equations (1.1a), (1.1b) and (1.1c). These solutions obey a boundary condition at $\tilde{r} \to \infty$, given in terms of a constant λ by

$$y_{11}(\tilde{r}) \sim 4\lambda K_0(\tilde{r}) \tag{2.1a}$$

for the 1:1 case,

$$y(\tilde{r}) \sim 6\lambda K_0(\tilde{r}) \tag{2.1b}$$

for both 1:2 and 2:1 cases.

The solutions are expressed as determinants of certain operators. For 1:1 salts, we have

$$y_{11}(\tilde{r}) = 2 \ln \det(1 + \lambda K_{\tilde{r}}) - 2 \ln \det(1 - \lambda K_{\tilde{r}}) \tag{2.2}$$

with $K_{\tilde{r}}$ an integral operator on $\mathbb{R}^+$ with kernel

$$K_{\tilde{r}}(u, v) = \frac{\exp(-\tilde{r}(u + u^{-1})/2)}{u + v}. \tag{2.3}$$

In the 1:2 case the solution reads

$$y_{12}(\tilde{r}) = \ln \det(1 - \lambda K_{\tilde{r}}^{(0)}) - \ln \det(1 - \lambda K_{\tilde{r}}^{(2)}) \tag{2.4}$$

while in the 2:1 situation it is

$$y_{21}(\tilde{r}) = \ln \det(1 + \lambda K_{\tilde{r}}^{(2)}) - \ln \det(1 + \lambda K_{\tilde{r}}^{(1)}) \tag{2.5}$$

where

$$K_{\tilde{r}}^{(0)} = (\zeta - \zeta^2)O_{\tilde{r}}^{(1)} + (\zeta^2 - \zeta)O_{\tilde{r}}^{(2)} \tag{2.6a}$$

$$K_{\tilde{r}}^{(1)} = (\zeta^2 - 1)O_{\tilde{r}}^{(1)} + (\zeta - 1)O_{\tilde{r}}^{(2)} \tag{2.6b}$$

$$K_{\tilde{r}}^{(2)} = (1 - \zeta)O_{\tilde{r}}^{(1)} + (1 - \zeta^2)O_{\tilde{r}}^{(2)}. \tag{2.6c}$$

Here $\zeta = e^{i2\pi/3}$ and $O_{\tilde{r}}^{(1)}$ and $O_{\tilde{r}}^{(2)}$ are integral operators on $\mathbb{R}^+$ with kernel

$$O_{\tilde{r}}^{(1)}(u, v) = \frac{\exp(-\tilde{r}[(1 - \zeta)u + (1 - \zeta^2)u^{-1}]/(2\sqrt{3}))}{-\zeta u + v} \tag{2.7}$$

and $O_{\tilde{r}}^{(2)}(u, v) = \overline{O_{\tilde{r}}^{(1)}(u, v)}$, the bar denoting complex conjugation. It can be shown [23] that $\det(1 - \lambda K_{\tilde{r}}^{(1)}) = \det(1 - \lambda K_{\tilde{r}}^{(0)})$ (making use of a change of variable $u \to u^{-1}$); thus from the solution to the case 1:2, y_{12}, one can obtain the solution for the case 2:1 as $y_{21} = -y_{12}$ with the change $\lambda \to -\lambda$, as previously announced.

To solve completely the problem we are interested in, we should impose the boundary condition (1.2) to express λ in terms of the bare charge ξ. Notice that the constant λ

introduced above is closely related to the effective charge ξ_{eff}. Indeed,

$$\xi_{\text{eff}} = 2\tilde{a}K_1(\tilde{a})\,\lambda \qquad (1\!:\!1) \tag{2.8a}$$

$$\xi_{\text{eff}} = 3\tilde{a}K_1(\tilde{a})\,\lambda \qquad (1\!:\!2) \tag{2.8b}$$

$$\xi_{\text{eff}} = 3\tilde{a}K_1(\tilde{a})\,\lambda \qquad (2\!:\!1). \tag{2.8c}$$

The determination of the effective charge in terms of the bare one is interesting *per se*, since it allows one to use, at large distances, the linear theory expression, provided that the bare charge is replaced by the effective one. Writing down the boundary condition (1.2) gives the bare charge as a function of the effective one. In the limiting case $\tilde{a} \to 0$, this relation may be inverted since the associated (so-called) connection problem was solved: knowing the large distance behaviour (2.1) of the solutions (2.2), (2.4) and (2.5), the short distance behaviour for $\tilde{r} \to 0$ follows [24]. The 1:1 and 1:2 cases for $a = 0$ were studied in detail by Tracy and Widom in [11]. The 2:1 situation, even for $a = 0$, was not explicitly considered in [11], although it can be obtained following the same lines as are exposed in [11].

The situation with $\tilde{a} \neq 0$ is analytically more difficult, but we will show below that useful expressions may nevertheless be derived there, that rely on accurate approximations for certain key quantities related to the parameter λ. These expressions allow one to fully cover the regime of thin cylinders and/or low salt $\tilde{a} < 1$, whereas the discussion of results valid at arbitrary salt content is deferred to section 6.

3. Asymptotic expansions

The results reported are obtained from the limit $\tilde{a} \to 0$ but turn out to be reliable for $\tilde{a} < 1$ (see below).

3.1. Short distance behaviour

The general results of [24] for the cylindrical Bullough–Dodd equation (which belongs to the Toda family and onto which the above asymmetric PB equation can be mapped) allow one to find the short distance asymptotics of $y(\tilde{r})$ given in equation (2.4) for 1:2 electrolytes. Allowing for negative values of ξ will therefore also provide the solution to the 2:1 case. Similarly, the 1:1 behaviour encoded in equation (2.2) follows from theorem 3 of [22] and its corollaries (in particular those derived in section IV.I of [22]).

It turns that the parameter λ plays an essential role here. Its position with respect to a threshold value λ_{c} discriminates two different small scale behaviours. The threshold values read

$$\lambda_{\text{c}}^{(1:1)} = \frac{1}{\pi} \tag{3.1a}$$

$$\lambda_{\text{c}}^{(1:2)} = \frac{1}{2\sqrt{3}\,\pi} \tag{3.1b}$$

$$\lambda_{\text{c}}^{(2:1)} = \frac{\sqrt{3}}{2\,\pi}. \tag{3.1c}$$

We will show that the condition $\lambda < \lambda_c$ is equivalent to $\xi < \xi_c$ where ξ_c is some threshold charge. In the limit $\kappa a = \tilde{a} \to 0$, ξ_c coincides with the known Manning parameter beyond which counterion condensation sets in:

$$\xi_{\text{Manning}}^{(1:1)} = 1 \tag{3.2}$$

$$\xi_{\text{Manning}}^{(1:2)} = 1/2 \tag{3.3}$$

$$\xi_{\text{Manning}}^{(2:1)} = 1. \tag{3.4}$$

However, as soon as $\tilde{a} \neq 0$, it will appear that ξ_c significantly differs from ξ_{Manning}. For $\lambda < \lambda_c$, we have [9, 22]

$$y_{11}(\tilde{r}) = -2A \ln \tilde{r} + 2 \ln B - 2 \ln \left[1 - \frac{B^2 \tilde{r}^{2-2A}}{16(1-A)^2} \right] + \mathcal{O}(\tilde{r}^{2+2A}) \qquad (1:1) \tag{3.5a}$$

$$y_{12}(\tilde{r}) = -2A \ln \tilde{r} + \ln B - \ln \left[1 - \frac{B^2 \tilde{r}^{2-4A}}{12(2A-1)^2} \right] + \mathcal{O}(\tilde{r}^{2+2A}) \qquad (1:2) \tag{3.5b}$$

$$y_{21}(\tilde{r}) = -2A \ln \tilde{r} + \ln B - 2 \ln \left[1 - \frac{\tilde{r}^{2-2A} B}{24(1-A)^2} \right] + \mathcal{O}(\tilde{r}^{2+4A}) \qquad (2:1) \tag{3.5c}$$

where A is a function of λ, see equations (3.11) and (3.13) below, and

$$B = 2^{3A} \frac{\Gamma\left((1+A)/2\right)}{\Gamma\left((1-A)/2\right)} \qquad (1:1) \tag{3.6a}$$

$$B = 3^{3A} 2^{2A} \frac{\Gamma\left((1+A)/3\right) \Gamma\left((2+2A)/3\right)}{\Gamma\left((2-A)/3\right) \Gamma\left((1-2A)/3\right)} \qquad (1:2) \tag{3.6b}$$

$$B = 3^{3A} 2^{2A} \frac{\Gamma\left((2+A)/3\right) \Gamma\left((1+2A)/3\right)}{\Gamma\left((1-A)/3\right) \Gamma\left((2-2A)/3\right)} \qquad (2:1). \tag{3.6c}$$

Here Γ is the Euler Gamma function.

On the other hand, for $\lambda > \lambda_c$ (or equivalently $\xi > \xi_c$), the short distance behaviour is characterized by a parameter $\mu > 0$ and we have

$$\mathrm{e}^{-y_{11}/2} \simeq \frac{\tilde{r}}{4\mu} \sin\left[-2\mu \log(\tilde{r}) - 2\mu \, \mathcal{C}^{(1:1)} \right] \tag{3.7a}$$

$$\mathrm{e}^{-y_{12}} \simeq \frac{\tilde{r}}{3\sqrt{3}\,\mu} \sin\left[-3\mu \log(\tilde{r}) - 3\mu \, \mathcal{C}^{(1:2)} \right] \tag{3.7b}$$

$$\mathrm{e}^{-y_{21}/2} \simeq \frac{\sqrt{2}\tilde{r}}{3\sqrt{3}\,\mu} \sin\left[-\frac{3}{2}\mu \log(\tilde{r}) - \frac{3}{2}\mu \, \mathcal{C}^{(2:1)} \right]. \tag{3.7c}$$

For the sake of notational simplicity, we do not explicitly mention that μ depends on the situation 1:1, 1:2 or 2:1 considered. The constants $\mathcal{C}$ appearing above are defined as

$$\mathcal{C}^{(1:1)} = \gamma - 3 \log 2 \simeq -1.502 \tag{3.8}$$

$$\mathcal{C}^{(1:2)} = \gamma - \tfrac{1}{3}\log 2 - \tfrac{3}{2}\log 3 \simeq -1.301 \tag{3.9}$$

$$\mathcal{C}^{(2:1)} = \gamma - \log 2 - \tfrac{3}{2}\log 3 \simeq -1.763 \tag{3.10}$$

where $\gamma \simeq 0.5772\ldots$ is the Euler constant. We emphasize that expressions (3.7) do not have the same status of mathematical rigour as their counterparts (3.5) valid for $\lambda < \lambda_c$, as appears in appendix B. The constants $\mathcal{C}$ in (3.7) arise from the linearization of a μ dependent function, which is justified from a practical point of view since for physically relevant situations, μ is small enough to allow for the corresponding Taylor expansions. For the exact expressions see appendix B.

We note here that the relation between surface potential and surface charge follows from the expressions given in the present section. At this point, the electric potential depends on a parameter A for $\lambda < \lambda_c$ or on a parameter μ for $\lambda > \lambda_c$. These two parameters are related to the bare reduced charge ξ of the cylindrical polyion through the boundary condition (1.2). Before clarifying this relation, we make precise the connection between small $\tilde{r}$ and large $\tilde{r}$ behaviour.

3.2. Connecting small and large scale features

For 1:1 electrolytes, the connection problem was solved in [9, 22], with the result

$$\lambda = \frac{1}{\pi} \sin\left(\frac{\pi A}{2}\right) \qquad \text{for } \lambda < \pi^{-1} \quad (\text{or } \xi < \xi_c) \tag{3.11}$$

$$\lambda = \frac{1}{\pi} \cosh(\pi\mu) \qquad \text{for } \lambda > \pi^{-1} \quad (\text{or } \xi > \xi_c). \tag{3.12}$$

Since λ is related to the effective charge which governs the far field behaviour (see (2.8)), the above expressions realize an interesting connection between small and large $\tilde{r}$ features.

For asymmetric electrolytes and $\lambda < \lambda_c$

$$A = -\frac{1}{4} + \frac{3}{2\pi} \arcsin\left(\frac{1}{2} + \frac{\lambda}{2\lambda_c}\right) \qquad (1:2) \tag{3.13a}$$

$$A = \frac{1}{4} + \frac{3}{2\pi} \arcsin\left(-\frac{1}{2} + \frac{3\lambda}{2\lambda_c}\right) \qquad (2:1). \tag{3.13b}$$

In these two expressions, the values of λ_c differ ($\lambda_c^{(2:1)} = 3\lambda_c^{(1:2)}$; see (3.1)) in such a way that expressing A as a function of $\lambda_c^{(1:2)}$ in both cases would provide the same expression, but a change in sign in A and in λ. This reflects the original symmetry of 1:2 and 2:1 situations, when ξ is allowed to change sign. This symmetry is broken here by the choice $\xi > 0$ in both cases, which illustrates the practical difference between them.

From a more formal point of view, the expressions (3.11) and (3.13) hold even for complex parameters, provided by

$$\lambda \notin (-\infty, -\lambda_c^{(1:1)}] \cup [\lambda_c^{(1:1)}, \infty) \qquad (1:1) \tag{3.14a}$$

$$\lambda \notin (-\infty, -\lambda_c^{(2:1)}] \cup [\lambda_c^{(1:2)}, \infty) \qquad (1:2) \tag{3.14b}$$

$$\lambda \notin (-\infty, -\lambda_c^{(1:2)}] \cup [\lambda_c^{(2:1)}, \infty) \qquad (2:1). \tag{3.14c}$$
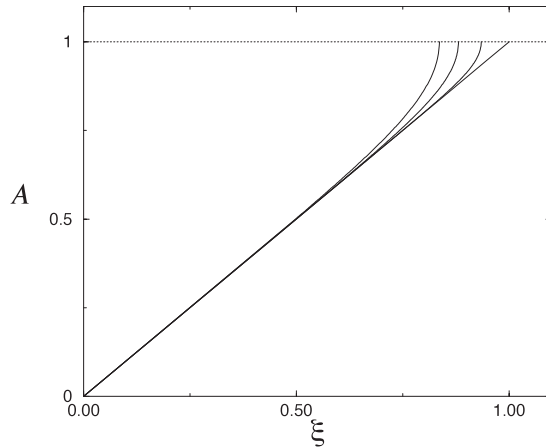
Figure 1. Small scale exponent A (relevant for $\lambda < \lambda_c$) as a function of bare charge for a 1:1 salt. Four salinities are displayed: from left to right, $\tilde{a} = 10^{-2}$, 10^{-3}, 10^{-6} and 0^+, the latter coinciding with the first bisectrix. The values of ξ where $A = 1$ correspond to an end point which defines the threshold bare charge ξ_c.

Alternatively, for $\lambda > \lambda_c$, we have

$$\frac{\lambda}{\lambda_c} + 1 = 2\cosh(\pi\mu) \qquad (1{:}2) \tag{3.15a}$$

$$\frac{3\lambda}{\lambda_c} - 1 = 2\cosh(\pi\mu) \qquad (2{:}1). \tag{3.15b}$$

3.3. Applying the boundary condition at polyion contact

In order to have a closed problem, we need to impose the boundary condition (1.2) at $\tilde{r} = \tilde{a}$ which relates A to ξ (and therefore λ to ξ from the connection formulae) if $\lambda < \lambda_c$ and similarly relates μ to ξ if $\lambda > \lambda_c$.

A straightforward computation gives in the 1:1 situation

$$\xi = A - \frac{(2 - 2A)(\kappa a)^{2-2A}}{16(1 - A)^2 B^2 - (\kappa a)^{2-2A}} \tag{3.16}$$

$$(\xi - 1)\tan\left[2\mu\log(\kappa a/8) + 2\mu\gamma\right] = 2\mu \tag{3.17}$$

where it is understood that the first line holds for $\lambda < \lambda_c$ while the second is relevant for $\lambda > \lambda_c$, in which case μ is the smallest positive root of the equation. Here again, γ denotes the Euler constant. The dependence of μ and A upon ξ is shown in figures 1 and 2.

In addition for the 1:2 situation, we get

$$\xi = A - \frac{(1 - 2A)(\kappa a)^{2-4A}B^2}{12(2A - 1)^2 - B^2(\kappa a)^{2-4A}} \tag{3.18}$$

$$(2\xi - 1)\tan\left[3\mu\log(\kappa a) + 3\mu\,\mathcal{C}^{(1{:}2)}\right] = 3\mu \tag{3.19}$$
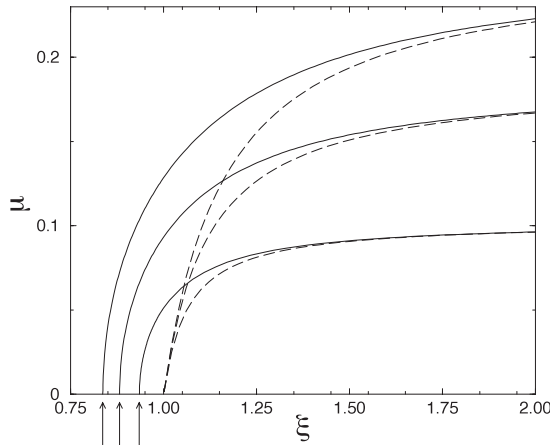
Figure 2. Small scale exponent μ relevant for $\lambda > \lambda_c = 1/\pi$ versus reduced bare charge (1:1 salt). The three curves correspond from left to right to $\tilde{a} = 10^{-2}$, 10^{-3} and 10^{-6}. The limit $\tilde{a} \to 0$ gives $\mu = 0$. The salt dependent threshold values ξ_c are shown by the arrows, which correspond to the end points where $A = 1$ in figure 1. The dashed curves correspond to approximation (4.13a).

while for the 2:1 case

$$\xi = A - \frac{2(1-A)(\kappa a)^{2-2A}B}{24(1-A)^2 - (\kappa a)^{2-2A}B} \tag{3.20}$$

$$(\xi - 1)\tan\left[\tfrac{3}{2}\mu \log(\kappa a) + \tfrac{3}{2}\mu\,\mathcal{C}^{(2:1)}\right] = \tfrac{3}{2}\,\mu \tag{3.21}$$

The values of B are given in (3.6).

At this point, we emphasize that the above expressions are not mathematically exact, since use was made of the asymptotic expansions given in section 3.1 to compute $\mathrm{d}y/\mathrm{d}\tilde{r}$ in (1.2). They nevertheless become asymptotically exact for $\kappa a = \tilde{a} \to 0$,[5] and will be shown to provide excellent results for the full range of thin cylinders $\tilde{a} < 1$.

Finally, it is important to remember that

$$A \to \xi_{\text{Manning}} \qquad \text{for } \lambda \to \lambda_c^- \quad (\text{or } \xi \to \xi_c^-) \tag{3.22}$$

$$\mu \to 0 \qquad \text{for } \lambda \to \lambda_c^+ \quad (\text{or } \xi \to \xi_c^+). \tag{3.23}$$

In the vicinity of the threshold ξ_c, it can be checked that $A - \xi_{\text{Manning}}$ and μ scale like $\sqrt{\xi - \xi_c}$, as may be expected from figures 1 and 2.

3.4. What are the associated threshold potentials and charges?

To understand the change of behaviour of the electrostatic potential below or above λ_c, it is instructive to compute the associated threshold charge ξ_c. There are several ways to

---

[5] In this respect, there is a further approximation in (3.17) compared to (3.16) since it relies on (3.7c), which is not exact. A similar remark holds for (3.19) or (3.21). It is however a simple task to get rid of this extra degree of approximation using the expressions given in appendix B. In any case, the resulting relation between ξ and μ is only asymptotically exact in the limit $\tilde{a} \to 0$, and resorting to the full expressions of appendix B brings very little improvement in terms of numerical accuracy.

perform such a computation, either from below taking the limit $\lambda \to \lambda_c^-$ and considering the relations between A and ξ, or from above ($\lambda \to \lambda_c^+$) manipulating μ. By construction (see appendix B for the details of the analytic continuation method used), these two routes provide the same short distance potentials, that read for the three different electrolytes

$$y_{11}(\tilde{r}) \overset{\lambda=\lambda_c}{=} -2\log\left(\frac{\tilde{r}}{2}\right) - 2\log\left[-\log(\tilde{r}) - \mathcal{C}^{(1:1)}\right] \tag{3.24a}$$

$$y_{12}(\tilde{r}) \overset{\lambda=\lambda_c}{=} -\log\left(\frac{\tilde{r}}{\sqrt{3}}\right) - \log\left[-\log(\tilde{r}) - \mathcal{C}^{(1:2)}\right] \tag{3.24b}$$

$$y_{21}(\tilde{r}) \overset{\lambda=\lambda_c}{=} -2\log\left(\frac{\tilde{r}}{\sqrt{6}}\right) - 2\log\left[-\log(\tilde{r}) - \mathcal{C}^{(2:1)}\right]. \tag{3.24c}$$

Limiting ourselves to the region $\tilde{a} < 1$ (as for all the results reported in this section 3)) ensures here that the previous expressions are real. Equations (3.24a) and (3.24b) were already given in [9, 11, 22, 24] and are repeated here for the sake of completeness (expression (3.24b) appeared under number (3.2) with misprints in [11], where the notation 21 used there corresponds to our 1:2 case[6]).

From equations (3.24), it is straightforward to compute the integrated charge $q(r)$ in a cylinder of radius r which reads $q(\tilde{r}) = -(\tilde{r}/2)\,dy/d\tilde{r}$ from Gauss's law. Evaluating this expression at $\tilde{r} = \tilde{a}$, we recover (1.2), and hence the value of ξ associated with λ_c:

$$\xi_c^{(1:1)} = 1 + \frac{1}{\log(\kappa a) + \mathcal{C}^{(1:1)}} \tag{3.25a}$$

$$\xi_c^{(1:2)} = \frac{1}{2} + \frac{1}{2\log(\kappa a) + 2\,\mathcal{C}^{(1:2)}} \tag{3.25b}$$

$$\xi_c^{(2:1)} = 1 + \frac{1}{\log(\kappa a) + \mathcal{C}^{(2:1)}} \tag{3.25c}$$

where the constants $\mathcal{C}$ are given in (3.8). We will see in section 4.1 that these threshold values, which discriminate $\lambda < \lambda_c$ behaviour from that at $\lambda > \lambda_c$, can be associated with the phenomenon of counterion condensation.

Expressions (3.25) correspond to the leading order behaviour of ξ_c and may be improved from the accurate expressions obtained in [22, 24]. In the 1:1 case, inclusion of the so far omitted dominant correction leads to

$$e^{-y_{11}/2} = \frac{\tilde{r}}{2}\,\Omega(\tilde{r}) + \frac{\tilde{r}^5\,\Omega(\tilde{r})}{2^9} + \mathcal{O}\left(\tilde{r}^5\log^2(\tilde{r})\right), \tag{3.26}$$

with

$$\Omega(\tilde{r}) = -\log(\tilde{r}) - \mathcal{C}^{(1:1)}. \tag{3.27}$$

Equation (3.24a) corresponds to truncating the right-hand side of (3.26) after the first term. The integrated charge $q(r)$ associated to (3.26) reads, including only the dominant correction to the $q(r)$ leading to (3.25a),

$$q(\tilde{r}) = 1 - \frac{1}{\Omega(\tilde{r})} + \frac{\tilde{r}^4\,\Omega^2(\tilde{r})}{16} + \mathcal{O}\left(\tilde{r}^3\,\Omega^3(\tilde{r})\right). \tag{3.28}$$

---

[6] We also note that references [9, 10] suffer from several typographic errors that make detailed comparison quite difficult.

From $q(\tilde{a}) = \xi$, we get that the error made in (3.25a)—which corresponds to the first two terms on the right-hand side of (3.28) evaluated at $\tilde{r} = \tilde{a}$—is of order $\tilde{a}^4(\log \tilde{a})^2$. More quantitatively, the terms neglected in (3.25a) are below 2×10^{-3} and are therefore irrelevant given that the term in $1/\log \tilde{a}$ in (3.25a) may be of order 0.1 or larger under reasonable salt conditions. A similar analysis could be performed to improve over expressions (3.25b) and (3.25c).

Finally, note that exactly at $\xi = \xi_c$, effective charges take a particularly simple form (making use of equations (2.8) and (3.1)) since then $\lambda = \lambda_c$.

4. A few limiting cases

4.1. $a = 0$ and arbitrary ξ

It is instructive to discuss first the case $a = 0$ (at fixed $\kappa > 0$) where the analytical solutions take simple forms and λ can be found explicitly. From equations (3.16), (3.18) or (3.20) we find $A = \xi$ and

$$\lambda = \frac{1}{\pi} \sin \frac{\pi \xi}{2} \qquad (1{:}1) \tag{4.1a}$$

$$\lambda = \frac{1}{2\sqrt{3}\pi} \left[2 \sin \left(\frac{2\pi}{3} \left(\xi + \frac{1}{4} \right) \right) - 1 \right] \qquad (1{:}2) \tag{4.1b}$$

$$\lambda = \frac{1}{2\sqrt{3}\pi} \left[2 \sin \left(\frac{2\pi}{3} \left(\xi - \frac{1}{4} \right) \right) + 1 \right] \qquad (2{:}1). \tag{4.1c}$$

From these results we obtain the effective charge of the rod. For $a = 0$, we simply have (see equation (2.8)) $\xi_{\mathrm{eff}} = 2\lambda$ (1:1) and $\xi_{\mathrm{eff}} = 3\lambda$ (1:2) or (2:1), and thus

$$\xi_{\mathrm{eff}} = \frac{2}{\pi} \sin \frac{\pi \xi}{2} \qquad (1{:}1) \tag{4.2a}$$

$$\xi_{\mathrm{eff}} = \frac{\sqrt{3}}{2\pi} \left[2 \sin \left[\frac{2\pi}{3} \left(\xi + \frac{1}{4} \right) \right] - 1 \right] \qquad (1{:}2) \tag{4.2b}$$

$$\xi_{\mathrm{eff}} = \frac{\sqrt{3}}{2\pi} \left[2 \sin \left[\frac{2\pi}{3} \left(\xi - \frac{1}{4} \right) \right] + 1 \right] \qquad (2{:}1). \tag{4.2c}$$

Equations (4.2a) and (4.2b) may be found in [9] and [11]. These formulae are valid only if the conditions (3.14) on λ are satisfied. Given that, for $a = 0$, the threshold charges (3.25) read

$$\xi_c^{(1:1)} = \xi_{\mathrm{Manning}}^{(1:1)} = 1 \tag{4.3a}$$

$$\xi_c^{(1:2)} = \xi_{\mathrm{Manning}}^{(1:2)} = \tfrac{1}{2} \tag{4.3b}$$

$$\xi_c^{(2:1)} = \xi_{\mathrm{Manning}}^{(2:1)} = 1 \tag{4.3c}$$

expressions (4.2) hold provided

$$\xi < 1 \qquad (1:1) \qquad\qquad (4.4a)$$

$$\xi < 1/2 \qquad (1:2) \qquad\qquad (4.4b)$$

$$\xi < 1 \qquad (2:1) \qquad\qquad (4.4c)$$

or, in the most general case allowing for negative values of the bare charge,

$$-1 < \xi < 1 \qquad (1:1) \qquad\qquad (4.5a)$$

$$-1 < \xi < 1/2 \qquad (1:2) \qquad\qquad (4.5b)$$

$$-1/2 < \xi < 1 \qquad (2:1). \qquad\qquad (4.5c)$$

We recover here the Onsager–Manning–Oosawa criterion for counterion condensation [2, 3, 9, 10, 13, 15, 25]. Strictly speaking, if ξ does not satisfy (4.4) there is no physical solution of the Poisson–Boltzmann equation for $a = 0$. As explained in [2], if the bare charge ξ is above the Manning–Oosawa threshold given in equations (4.4), the Boltzmann factor of the interaction between the rod and a counterion is not integrable at short distances, and thus would lead to a collapse between the macroion and the counterions. The situation is similar to the one in the theory of two-dimensional Coulomb systems [28, 29], with logarithmic interaction, where a system of point particles is stable only if the charge of the particles is small enough so that the Boltzmann factor of the interaction between two oppositely charged particles is integrable. Otherwise only a system with hard core particles (or with other short distance regularization of the Coulomb potential) is stable.

For the 1:2 electrolyte, the value $\xi = \xi_{\mathrm{Manning}}^{(1:2)} = 1/2$ corresponds to Manning–Oosawa threshold [2, 3]. Beyond the threshold ($\xi \geq 1/2$), the effective charge ξ_{eff} attains its saturation value, $\xi_{\mathrm{eff}}^{\mathrm{sat}} = \sqrt{3}/(2\pi) \simeq 0.275$. One may check that in the linear regime (weak charges, $\xi \ll 1$), ξ_{eff} and ξ coincide, as they should. For the 2:1 electrolyte, the Manning–Oosawa threshold is for $\xi = \xi_{\mathrm{Manning}}^{(2:1)} = 1$ and beyond this threshold the effective saturated charge is given by $\xi_{\mathrm{eff}}^{\mathrm{sat}} = 3\sqrt{3}/(2\pi)$; it is three times larger than in the 1:2 case. In the symmetric 1:1 electrolyte case, the Manning–Oosawa threshold is for $\xi = \xi_{\mathrm{Manning}}^{(1:1)} = 1$ and the corresponding effective saturated charge is $\xi_{\mathrm{eff}}^{\mathrm{sat}} = 2/\pi \simeq 0.636$. We note that this result is in harmony with exact bounds derived by Odijk in [30]: $0.59 < \xi_{\mathrm{eff}}^{\mathrm{sat}} < 0.67$.

This analysis clarifies the relationship between two different notions, the Manning–Oosawa threshold for counterion condensation and the notion of effective charge. The key point here is that the Manning–Oosawa threshold ξ_{Manning} for the bare charge is different from the value of the saturated effective charge $\xi_{\mathrm{eff}}^{\mathrm{sat}}$. The fact that $\xi_{\mathrm{eff}}^{\mathrm{sat}} < \xi_{\mathrm{Manning}}$ is of course a non-linear effect which means that even accounting correctly for counterion condensation, the remaining layer of 'uncondensed' or 'free' microions *cannot* be treated within a linearized (Debye–Hückel-like) theory. This exact result contrasts with common belief in the field, which possibly takes its roots in the work of Manning [2].

In figures 3 and 4, we compare the results of equations (4.2b) and (4.2c) for a 1:2 and 2:1 electrolyte, respectively, with numerical data, for two low values of κa. All numerical PB data have been obtained following the method discussed in [31]. One may conclude
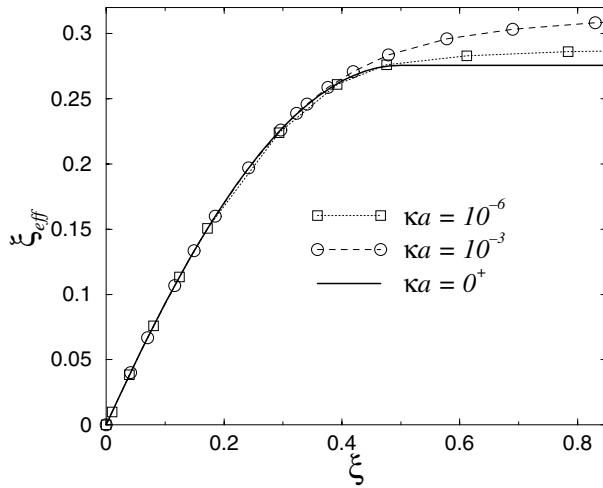
Figure 3. Effective versus bare line charge for an infinite charged rod (1:2 case). The analytical result (4.2*b*) valid in the low salt or thin rod limit $\kappa a \to 0$, shown by the thick continuous curve, is compared to the numerical solution of Poisson–Boltzmann theory for $\kappa a = 10^{-6}$ and $\kappa a = 10^{-3}$.
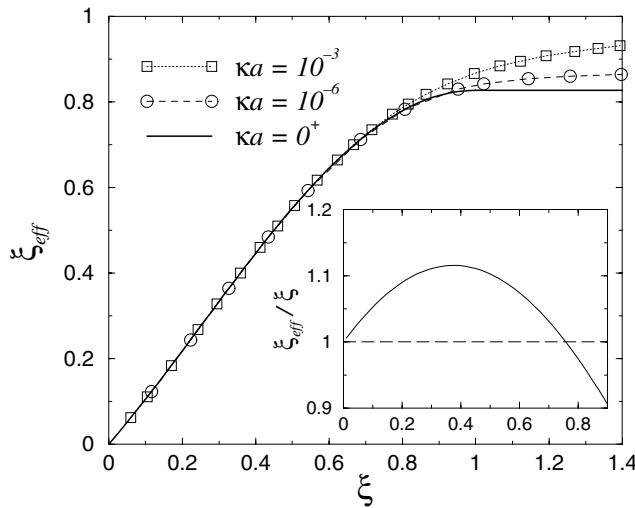

Figure 4. Same as figure 3 but for the 2:1 electrolyte. Inset: ξ_{eff}/ξ for small values of ξ. Notice the initial overshooting effect $\xi_{\text{eff}} > \xi$.

that the limiting behaviour $\kappa a \to 0$ is reached very slowly, in fact, logarithmically, as we will show below.

It is interesting to note in figure 4 that in the 2:1 electrolyte we have the overshooting effect, previously reported in [32], where the effective charge becomes larger than the bare charge for intermediate values of the latter. Indeed for $|\xi| \ll 1$, from equations (4.2), we have for a 2:1 electrolyte

$$\xi_{\text{eff}} = \xi + \frac{\pi \xi^2}{3\sqrt{3}} - \frac{2\pi^2 \xi^3}{27} + \mathcal{O}(\xi^4) \qquad (2:1) \qquad (4.6)$$

and for a 1:2 electrolyte

$$\xi_{\mathrm{eff}} = \xi - \frac{\pi \xi^2}{3\sqrt{3}} - \frac{2\pi^2 \xi^3}{27} + \mathcal{O}(\xi^4) \qquad (1:2). \tag{4.7}$$

The first deviation of the effective charge from linear behaviour is positive in the 2:1 case (overshooting effect) and negative in the 1:2 case (no overshooting). For a 1:1 electrolyte,

$$\xi_{\mathrm{eff}} = \xi - \frac{\pi^2}{24}\xi^3 + \mathcal{O}(\xi^5). \tag{4.8}$$

The first deviation of the effective charge from the bare one is of order ξ^3 (as in the case $\kappa a \gg 1$ [32]) and negative (thus no overshooting). There is no term in ξ^2 as opposed to the case for the charge asymmetric electrolytes 1:2 and 2:1. The physical origin of the overshooting effect lies in the fact that in the 2:1 case, the divalent coions are expelled further away in the double layer than the monovalent ones in the 1:1 situation, which results in a stronger electrostatic potential at large distances. Similarly, the screening for 1:2 electrolytes is more efficient since divalent counterions are available, which not only results in the fact that $\xi_{\mathrm{eff}} < \xi$, but also in the lower value of $\xi_{\mathrm{eff}}^{\mathrm{sat}}$. We therefore speculate that the overshooting effect is generic in a z:z' electrolyte, with coions of valency z larger than that of counterions (z').

4.2. $\xi \to 0$ and arbitrary $\tilde{a} < 1$

In the limit where $\xi \to 0$, the solution (1.3) becomes exact for all distances, and one has $\xi_{\mathrm{eff}}/\xi \to 1$, as was simply checked for $a = 0$ in section 4.1. At finite salt however, the requirement $\xi_{\mathrm{eff}}/\xi \to 1$ when $\xi \to 0$ provides quite a non-trivial benchmark for our analytical expressions. It turns that the results of sections 3.2 and 3.3 are not sufficient— at finite $\tilde{a}$—to show $\xi_{\mathrm{eff}}/\xi \to 1$. This is because in equations (3.5) we neglected terms of order $\tilde{r}^{2+2A}$ in the 1:1 and 1:2 cases and terms of order $\tilde{r}^{2+4A}$ in the 2:1 case. As $\xi \to 0$, we have $A \to 0$; thus these terms become of order r^2 and are of the same order of the last term in the logarithms of equations (3.5). Then, to properly compute the short distance asymptotics as $\xi \to 0$, we need the next order terms in equations (3.5). These can be easily obtained by replacing the small r asymptotics (3.5) into the Poisson–Boltzmann differential equation (1.1). For example for the 1:1 case, we obtain, if $A < 1$,

$$\mathrm{e}^{-y_{11}/2} = \frac{\tilde{r}^A}{B}\left[1 - \frac{\tilde{r}^2}{16}\left(\frac{B^2 \tilde{r}^{-2A}}{(1-A)^2} - \frac{\tilde{r}^{2A}}{B^2(1+A)^2}\right) + \mathcal{O}(\tilde{r}^{2(2+2A)})\right]. \tag{4.9}$$

Notice the expected symmetry in the two terms when one changes $A \to -A$ (in which, from the definition of B, gives $B \to B^{-1}$). Taking the limit $A \to 0$ we obtain

$$y_{11}(r) = -2A\left[\ln\frac{\tilde{r}}{2} + \gamma + \frac{\tilde{r}^2}{4}\left(\gamma + \ln\frac{\tilde{r}}{2} - 1\right)\right] + \mathcal{O}(\tilde{r}^4). \tag{4.10}$$

We recognize the small r expansion of the Bessel function $K_0(\tilde{r})$. On the other hand (3.11) says that for $A \to 0$, $A = 2\lambda = \xi_{\mathrm{eff}}/(\tilde{a}K_1(\tilde{a}))$. We conclude that the small r expansion (4.10) is the small r expansion of the linear solution (1.3) and that, clearly, imposing the boundary condition (1.2) at $r = a$ will yield $\xi = \xi_{\mathrm{eff}}$.

A similar conclusion is reached for the asymmetric cases. For the 2:1 case the small r expansion, for $A < 1$, reads

$$e^{-y_{21}/2} = \tilde{r}^A B^{-1/2}\left[1 - \frac{\tilde{r}^{2-2A}B}{24(1-A)^2} + \frac{\tilde{r}^{2+4A}}{24B^2(2A+1)^2} + \mathcal{O}(\tilde{r}^{2(2+4A)})\right] \quad (4.11)$$

while the one for y_{12} can be obtained from the preceding expression through the substitution $A \to -A$ and $B \to B^{-1}$. It can be directly verified that in the limit $A \to 0$, the asymptotics (4.11) yield again (4.10); that is the small r asymptotics of y_{12} and y_{21} are those of the Bessel function $K_0(\tilde{r})$, the solution of the linear problem.

4.3. $\xi = \xi_{\mathrm{Manning}}$ and arbitrary $\tilde{a} < 1$

It is in general not possible to find analytically the solution to the transcendental equations satisfied by the parameter μ, which quantifies the behaviour at short distances above the salt dependent threshold, i.e. for $\xi > \xi_{\mathrm{c}}$. However, if $\xi = \xi_{\mathrm{Manning}}$ (which is always beyond ξ_{c}), the relevant roots of equations (3.17), (3.19) and (3.21) read

$$\mu^{(1,1)} = -\frac{\pi}{4[\log \tilde{a} + \mathcal{C}^{(1:1)}]} \quad (4.12a)$$

$$\mu^{(1,2)} = -\frac{\pi}{6[\log \tilde{a} + \mathcal{C}^{(1:2)}]} \quad (4.12b)$$

$$\mu^{(2,1)} = -\frac{\pi}{3[\log \tilde{a} + \mathcal{C}^{(2:1)}]}. \quad (4.12c)$$

These expressions will be useful in section 5.

4.4. $\xi > \xi_{\mathrm{Manning}}$ and arbitrary $\tilde{a} < 1$

The limit of large enough ξ allows one to derive a useful approximation for μ, that will turn out to be important from a practical point of view. Coming back to equations (3.17), (3.19) and (3.21), we note that for diverging ξ, the arguments of the tangent functions should be close to $-\pi$, so that the tangent functions vanish, to be compatible with a finite value of μ. Expanding then the tangent to first order, we obtain

$$\mu^{(1,1)} \simeq -\frac{\pi}{2[\log \tilde{a} + \mathcal{C}^{(1:1)} - 1/(\xi - 1)]} \quad (4.13a)$$

$$\mu^{(1,2)} \simeq -\frac{\pi}{3[\log \tilde{a} + \mathcal{C}^{(1:2)} - 1/(2\xi - 1)]} \quad (4.13b)$$

$$\mu^{(2,1)} \simeq -\frac{2\pi}{3[\log \tilde{a} + \mathcal{C}^{(2:1)} - 1/(\xi - 1)]}. \quad (4.13c)$$

The domain of validity of these relations is estimated to be $\xi > \xi_{\mathrm{Manning}} + \mathcal{O}(1/\log \tilde{a})$, as may be observed in figure 2 in the 1:1 case. In the vicinity of ξ_{Manning} where (4.13) fails, one should resort to expressions (4.12). We finally note that when ξ diverges, μ saturates to a finite value (twice those reported in (4.12))

$$\mu_{\mathrm{sat}}^{(1,1)} = -\frac{\pi}{2[\log \tilde{a} + \mathcal{C}^{(1:1)}]} \quad (4.14a)$$

$$\mu_{\mathrm{sat}}^{(1,2)} = -\frac{\pi}{3[\log \tilde{a} + \mathcal{C}^{(1:2)}]} \quad (4.14b)$$

$$\mu_{\mathrm{sat}}^{(2,1)} = -\frac{2\pi}{3[\log \tilde{a} + \mathcal{C}^{(2:1)}]}. \quad (4.14c)$$

From equations (3.12) and (3.15) we conclude that λ also saturates: a corollary is that effective charges—directly related to λ through (2.8)—saturate, a generic feature of mean field theories [33].

5. Results at finite salt and discussion

The results reported in sections 3 and 4 are based on asymptotic expansions in the limit $\tilde{a} \to 0$. This limit is approached logarithmically slowly, so that finite $\tilde{a}$ corrections should always be important in practice. We now therefore address the question of the reliability of our expressions at finite salt, by confronting them with the numerical solution of the non-linear PB equation (1.1).

5.1. Counterion condensation and Manning radius

One of the most interesting features emerging here is that it is possible to generalize the notion of counterion condensation to finite salt systems. It is important however to emphasize here that condensation is not an all or nothing process, that would occur precisely at ξ_c. Instead, it is a gradually built up phenomenon. This is particularly true at finite salt density but already in the limit of vanishing salt $\kappa a \to 0$, it is noteworthy that non-linear effects play an important role for $\xi < \xi_c$, as revealed by the fact that $\xi_{\text{eff}}/\xi \neq 1$.

We concentrate here on a 1:1 salt, but the same analysis also holds for 1:2 and 2:1 salts. The value ξ_c discriminates between the short distance behaviours (3.5a) for $\xi < \xi_c$ and (3.7a) for $\xi > \xi_c$. As may be observed in figure 1, A is close to ξ except in the vicinity of the threshold charge ξ_c, so that to dominant order, y_{11} behaves as $-2\xi \log \tilde{r}$, which corresponds to the potential of a bare cylinder with reduced charge ξ, unaffected by screening. At $\xi = \xi_c$, the potential develops an additional $\log \log r$ term (see section 3.4) while for $\xi > \xi_c$, the behaviour stemming from (3.7a) is more complex. For high enough ξ (more precisely, for $\xi > \xi_{\text{Manning}} + |\mathcal{O}(1/\log \tilde{a})| > \xi_{\text{Manning}}$ (which is itself larger than ξ_c), one may resort to approximation (4.13) and after some manipulations, rewrite (3.7a) as

$$e^{-y_{11}/2} \overset{r \simeq a}{\simeq} \frac{\tilde{r}}{2} \left[\log \left(\frac{\tilde{r}}{\tilde{a}} \right) + \frac{1}{\xi - 1} \right]. \tag{5.1}$$

Here, we have used the fact that

$$2\mu \left(\log \tilde{r} + \mathcal{C}^{(1:1)} \right) = -\pi + 2\mu \log \left(\frac{r}{a} \right) + \frac{2\mu}{\xi - 1} \tag{5.2}$$

so that equation (5.1) holds for $\log(r/a) \ll \mathcal{O}(1/\mu)$. Equation (5.1) had already been derived by Ramanathan [7] (see also appendix A of [34]) and implies that to dominant order, the potential behaves like $-2 \log r$ at short distances, which corresponds to the bare potential of a polyion with $\xi = \xi_{\text{Manning}} = 1$, and is the fingerprint of counterion condensation. We also note that for high ξ, equation (5.1) yields a total concentration of ions close to the rod that is proportional to the square of the surface charge density, as in the planar case [35]. To complement the above results that assume $\xi > \xi_{\text{Manning}} + |\mathcal{O}(1/\log \tilde{a})|$, we also mention that for $\xi = \xi_{\text{Manning}}$ (i.e. above the threshold),

the results of section 4.3 yield

$$
e^{-y_{11}/2} \overset{r \simeq a}{\simeq} -\frac{\tilde{r}}{\pi} \left(\log \tilde{a} + \mathcal{C}^{(1:1)} \right). \tag{5.3}
$$

The dominant behaviour for y_{11} is therefore again $-2 \log r$. Finally, decreasing further ξ to investigate the regime where it is close to the threshold ξ_c (but still larger than ξ_c), one may take advantage of μ vanishing at $\xi = \xi_c$ to get equations (3.24)

$$
e^{-y_{11}/2} = -\frac{\tilde{r}}{2} \left(\log \tilde{r} + \mathcal{C}^{(1:1)} \right) \tag{5.4a}
$$

$$
e^{-y_{12}} = -\frac{\tilde{r}}{\sqrt{3}} \left(\log \tilde{r} + \mathcal{C}^{(1:2)} \right) \tag{5.4b}
$$

$$
e^{-y_{21}/2} = -\frac{\tilde{r}}{\sqrt{6}} \left(\log \tilde{r} + \mathcal{C}^{(2:1)} \right). \tag{5.4c}
$$

The dominant behaviour at small scales is again $y \simeq -2\xi_{\text{Manning}} \log \tilde{r}$, which is the unscreened potential created by a rod of reduced charge ξ_{Manning}. This is quite remarkable given $\xi_c < \xi_{\text{Manning}}$ since it holds in particular for a cylinder with ξ verifying $(\xi_c <)\xi < \xi_{\text{Manning}}$. Such a remark is nevertheless quite misleading since at finite values of κa, the requirement $r > a$ does not allow one to take the limit $r \to 0$ where the different leading and sub-leading contributions to the potential can be identified: 'corrections' to the 'leading' term are important. In other words, the full expression is required to approximate y in (5.4) and the 'dominant' term $-2\xi_{\text{Manning}} \log \tilde{r}$ is in practice a bad approximation.

Our analytical expressions identify a mathematical change in the behaviour of the electric potential at $\xi = \xi_c$, that may be considered as being associated with counterion condensation. Such a terminology may however be confusing since at finite $\tilde{a}$, no singularity signals the crossing of the threshold value ξ_c. This restriction should be borne in mind. Of particular interest is the condensate structure, completely encoded in equations (3.7), and in particular the condensate thickness [13, 15]. Its definition is necessarily arbitrary. The so-called Manning radius is often considered when it comes to quantifying the condensate size. It is defined as the distance r_m where the integrated charge $q(r) = -(r/2)\,\mathrm{d}y/\mathrm{d}r$ equals ξ_{Manning}. Since we have seen that $\xi_c < \xi_{\text{Manning}}$, it is clear that such a criterion is inoperant for $\xi_c < \xi < \xi_{\text{Manning}}$, which constitutes quite a deficiency, but the corresponding value r_m nevertheless exhibits remarkable features within its domain of definition $\xi > \xi_{\text{Manning}}$. We first compute $q(r)$, that follows directly from equations (3.7):

$$
q^{(1:1)}(r) = 1 + 2\mu \tan \left[-2\mu \log \left(\frac{r}{r_{\text{m}}^{(1:1)}} \right) \right] \tag{5.5a}
$$

$$
q^{(1:2)}(r) = \frac{1}{2} + \frac{3\mu}{2} \tan \left[-3\mu \log \left(\frac{r}{r_{\text{m}}^{(1:2)}} \right) \right] \tag{5.5b}
$$

$$
q^{(2:1)}(r) = 1 + \frac{3\mu}{2} \tan \left[-\frac{3\mu}{2} \log \left(\frac{r}{r_{\text{m}}^{(2:1)}} \right) \right]. \tag{5.5c}
$$

with

$$\kappa r_{\mathrm{m}}^{(1:1)} = \exp\left(-\mathcal{C}^{(1:1)} - \frac{\pi}{4\mu}\right) \tag{5.6a}$$

$$\kappa r_{\mathrm{m}}^{(1:2)} = \exp\left(-\mathcal{C}^{(1:2)} - \frac{\pi}{6\mu}\right) \tag{5.6b}$$

$$\kappa r_{\mathrm{m}}^{(2:1)} = \exp\left(-\mathcal{C}^{(2:1)} - \frac{\pi}{3\mu}\right). \tag{5.6c}$$

In these expressions, one observes that $q(r) = \xi_{\mathrm{Manning}}$ for $r = r_m$, which means that the r_m appearing in (5.5) are by definition Manning radii. When $\xi = \xi_{\mathrm{Manning}}$, then by definition the Manning radius should coincide with the polyion radius a. This is indeed the case here, as a consequence of equations (4.12). For large enough ξ, we obtain an expression in closed form from approximation (4.13):

$$\kappa r_{\mathrm{m}}^{(1:1)} \simeq 2\sqrt{2\kappa a}\,\exp\left(-\frac{\gamma}{2} - \frac{1}{2(\xi-1)}\right) \tag{5.7a}$$

$$\kappa r_{\mathrm{m}}^{(1:2)} \simeq \frac{3^{3/4}}{2^{1/3}}\sqrt{2\kappa a}\,\exp\left[-\frac{\gamma}{2} - \frac{1}{2(2\xi-1)}\right] \tag{5.7b}$$

$$\kappa r_{\mathrm{m}}^{(2:1)} \simeq 3^{3/4}\sqrt{2\kappa a}\,\exp\left[-\frac{\gamma}{2} - \frac{1}{2(\xi-1)}\right]. \tag{5.7c}$$

In the cell model, the previous definition

$$q(r_m) = \xi_{\mathrm{Manning}} \tag{5.8}$$

offers a geometric construction for computing r_m: $q(r)$ plotted as a function of $\log r$ displays an inflection point at $r = r_m$ (see [13] where it was also shown that this criterion could be extended beyond the mean field and used in molecular dynamics simulations to define a fraction of condensed ions). From the functional form of equations (5.5)—with a shifted tangent as a function of $\log r$, i.e. the same form as in the salt free cell model case—we see that a similar inflection point criterion holds here. This will be illustrated further in section 5.3.

For a 1:1 electrolyte, (5.7a) is precisely the result obtained in [15]. The present work therefore makes precise the domain of validity of this expression, and offers with (5.6a) supplemented with (3.17) a better approximation (see figure 5). By construction, the accuracy of our expressions improves upon decreasing $\tilde{a}$. To test the worst cases, we therefore chose a relatively 'high' value $\tilde{a} = 0.01$ in figure 5, where the agreement is seen to be very good, while (5.7a) fails when ξ is too close to $\xi_{\mathrm{Manning}} = 1$. Figure 6 illustrates the effect of increasing salinity and displays the results associated with three values of $\tilde{a}$. It is observed that at high ξ, the analytical predictions deviate all the more from the numerical results computed for PB theory as $\tilde{a}$ is increased. For the highest value $\tilde{a} = 0.3$ of figure 6, the error made when $\xi \to \infty$ is of the order of 30%. It also appears that even at relatively high $\tilde{a}$, the analytical prediction is reliable for low ξ (bearing in mind that ξ must be larger than ξ_{Manning} to allow for the definition of r_m through equation (5.8)). For completeness, we present results for the 1:2 case as well in figure 7, changing $\tilde{a}$ at fixed charge $\xi = 0.55$ which is just above the value $\xi_{\mathrm{Manning}} = 1/2$. The results at saturation are also reported (dashed line and squares). One needs to push $\tilde{a}$ beyond 0.1 to notice a
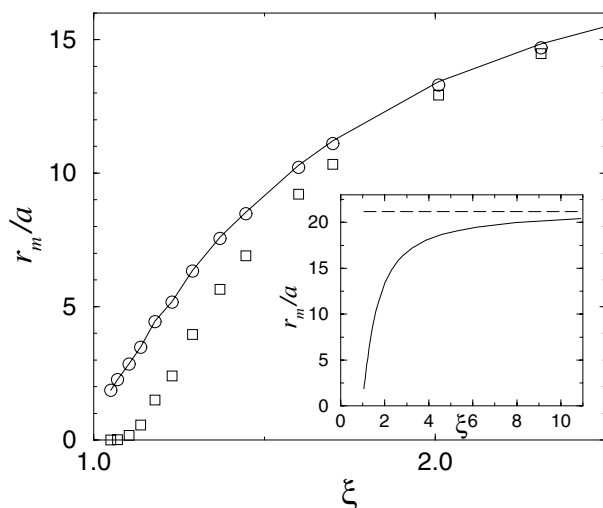
Figure 5. Manning radius r_m as defined from equation (5.8) versus reduced bare charge ξ, for a 1:1 salt with $\kappa a = 10^{-2}$ (a is the polyion radius). The continuous curve shows the results obtained from the numerical solution of PB equation, while the circles stand for expression (5.6a) where μ is the smallest positive root of (3.17) (see figure 2 for a plot of μ as a function of bare charge). The squares indicate the prediction (5.7a) (see the dashed line in figure 2 for the associated μ) which becomes asymptotically correct for large ξ. The inset displays the corresponding charge regime, where r_m/a saturates at high ξ to the value $2\sqrt{2/\tilde{a}}\exp(-\gamma/2)$ indicated by the dashed horizontal line.

difference between (5.6b) and the numerical PB result (see the inset). Figure 7 illustrates how finite salt effects influence the scaling exponent α in the relation $\kappa r_m \propto (\kappa a)^\alpha$. If $\xi > \xi_{\text{Manning}} + |\mathcal{O}(1/\log \tilde{a})|$, that is at high enough ξ or low enough $\tilde{a}$, we have $\alpha = 1/2$ as dictated by equations (5.7) and evidenced by the dotted line in the main graph. If on the other hand one sits in the region $\xi_{\text{Manning}} < \xi < \xi_{\text{Manning}} + |\mathcal{O}(1/\log \tilde{a})|$, the exponent α changes continuously, and increasing $\tilde{a}$ at fixed ξ drives the system toward the regime $\alpha = 1$, a feature—visible for the data at $\xi = 0.55$ in figure 7—which simply reflects the fact that $r_m \to a$. Finally, we emphasize that the behaviours in all three 1:1, 1:2 and 2:1 situations are qualitatively very similar so that the conclusions reached and phenomena observed are transferable from one situation to another.

The inflection point feature stemming from (5.8) has the merit of unifying the present infinite dilution/finite salt phenomenology with the finite density/vanishing salt situation of the cell model. It should be kept in mind however that (5.8) does not allow one to define a Manning radius for $\xi_c < \xi < \xi_{\text{Manning}}$, where the condensation phenomenon is already present, *at least from a mathematical point of view* with a change in the short distance behaviour of $y(r)$. In addition the scaling $r_m \propto (a/\kappa)^{1/2}$ valid for large enough ξ (see (5.7)) is definition dependent. An alternative to (5.8) could be defining a characteristic radius of the condensate through $q(r^*) = \xi_c$. Making use of (4.13) then implies that for a 1:1 salt $\kappa r^* \propto (\kappa a)^\alpha$ with $\alpha = (\arctan \pi)/\pi \simeq 0.402$ instead of $\alpha = 1/2$ in (5.7). As (4.13), this is limited to high enough ξ. For $\xi = 1$, the results of section 4.3 allow for an analytical computation of r^* and yield $\alpha = (2/\pi)\arctan(\pi/2) \simeq 0.639$.
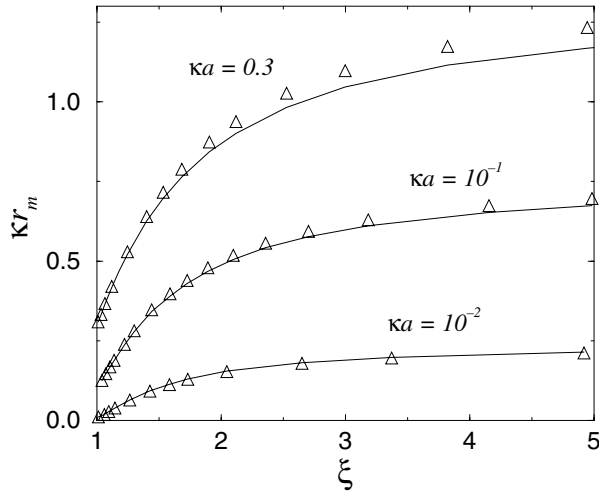
Figure 6. The Manning radius r_m versus the reduced bare charge ξ for a 2:1 salt, for different values of κa. The continuous curve shows the prediction of equation (5.6c) while the triangles correspond to the numerical solution of PB theory.
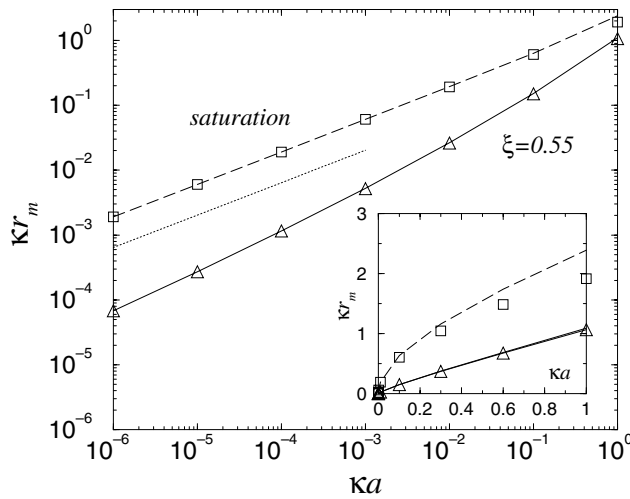

Figure 7. Manning radius as a function of salinity $\tilde{a}$ for two different charges and a 1:2 salt. The symbols show the prediction of equation (5.6b) (triangles for $\xi = 0.55$ and squares in the saturation limit corresponding to $\xi \to \infty$). The continuous and dashed lines display the corresponding numerical solution of PB theory. The dotted line is a guide for the eye indicating a slope $\alpha = 1/2$. The inset shows the same data on a linear scale.

Our expressions also allow one to discuss several quantities that directly follow from the electric potential, such as the Bjerrum radius r_B considered in [36] and defined as the locus of an inflection point in the integrated counterion density when plotted as a function of radial distance. For 1:1 and 2:1 salts, this definition implies $q(r_B) = 1/2$ while in the 1:2 case, we have $q(r_B) = 1/4$. Making use of equations (5.5) provides a transcendental equation from which r_B follows.
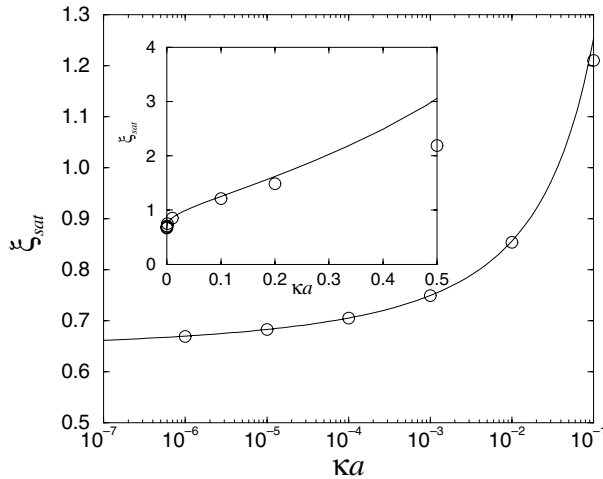
Figure 8. Effective linear charge density at saturation, ξ_{sat} as a function of the radius $\tilde{a}$ of the rod for a symmetric 1:1 electrolyte. The full line is the analytical expression (5.9a); the circles have been obtained by solving numerically the Poisson–Boltzmann equation. The inset shows the same data on a linear scale.

5.2. Effective charges

Of particular interest for describing interactions at large distances (typically $r > \kappa^{-1}$ as will be discussed in section 5.3) is the effective charge defined from the far field asymptotics (1.3). This quantity is given by equations (2.8) where λ follows from the expressions given in sections 3.2 and 3.3. The results pertaining to the limit $\tilde{a} \to 0$ have been given in section 4.1, but it is also possible to derive closed form relations in the saturation limit $\xi \to \infty$ where μ is given by (4.14). We therefore have (denoting $\xi_{\mathrm{eff}}^{\mathrm{sat}}$ by ξ_{sat})

$$\xi_{\mathrm{sat}}^{(1:1)} = \tilde{a} K_1(\tilde{a}) \frac{2}{\pi} \left[\cosh \left(\frac{\pi^2}{2[\log \tilde{a} + \mathcal{C}^{(1:1)}]} \right) \right] \tag{5.9a}$$

$$\xi_{\mathrm{sat}}^{(1:2)} = \tilde{a} K_1(\tilde{a}) \frac{\sqrt{3}}{\pi} \left[\cosh \left(\frac{\pi^2}{3[\log \tilde{a} + \mathcal{C}^{(1:2)}]} \right) - \frac{1}{2} \right] \tag{5.9b}$$

$$\xi_{\mathrm{sat}}^{(2:1)} = \tilde{a} K_1(\tilde{a}) \frac{\sqrt{3}}{\pi} \left[\cosh \left(\frac{2 \pi^2}{3[\log \tilde{a} + \mathcal{C}^{(2:1)}]} \right) + \frac{1}{2} \right] . \tag{5.9c}$$

Figures 8 and 9 show that the analytical expressions (5.9) are in good agreement with the numerical results for $\kappa a = \tilde{a} < 0.1$. For $\tilde{a} > 0.1$, deviations become apparent (see the inset of figure 8). We will propose in section 6 an alternative approach that covers the whole range of κa.

We have also checked that the effective charges are correctly described by the analytical predictions of section 3, not only in the saturation regime but also for arbitrary values of the charge ξ provided $\tilde{a} < 0.1$.
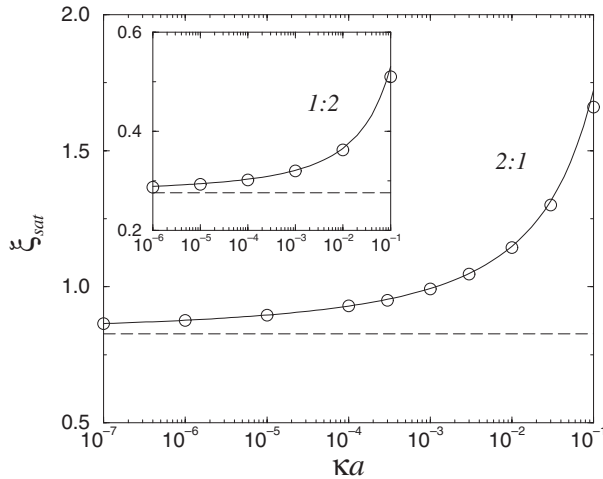
22

Figure 9. Same as the main graph of figure 8 but for 1:2 and 2:1 electrolytes. The analytical expressions shown by the lines are those of equations (5.9b) and (5.9c). The limiting values for $\kappa a \to 0^+$ are shown by the dashed lines.

5.3. Electric potential

So far, we have focused on several scalar quantities characterizing the electric potential, and thus the ionic distribution. It is also instructive to compare the analytical potentials to their 'exact' PB counterparts. When $\xi > \xi_{\rm c}$, the relevant small scale expressions are those of equations (3.7). We take the 2:1 situation as an illustrative example. As expected from the results of section 5.2, figures 10 and 11 show that the far field behaviour is well captured by (1.3), and it also appears that such an expression may be used in practice for $\kappa r > 1$. On the other hand, expansion (3.7c) is very accurate at short distances, and may be extended up to κr of order 1. For the low values of κa such as that of figure 10, expansion (3.7c) produces the correct potential with an exceptional accuracy for several orders of magnitude in r. For higher values of κa, the short distance expansion (3.7c) is still useful and reliable up to κr of order unity (see figure 11). To illustrate the improvement over previous expansions, we come back to the 1:1 case in figure 12 and compare our formula with the classic one of Ramanathan [7], recalled in (5.1) and re-derived in the present work. Once the potential is known, one can compute the integrated charge $q(r) = -(1/2)r \, {\rm d}y/{\rm d}r$, displayed in figure 13. The coincidence between the q versus $\log r$ inflection point and the Manning radius may be observed in the inset. The integrated charge—shown by the dotted line—following from (5.1) cannot reproduce such a feature, and we also observe that the most significant decay of $q(r)$ from its initial value (ξ as required by Gauss theorem, i.e. 25 in figure 13) to unity occurs on a much smaller scale than the Manning radius.

6. Effective charge at saturation and the largest eigenvalue of the operators $K_{\tilde{a}}$

The results of the previous sections are broadly speaking restricted to the regime $\kappa a < 1$. For the specific problem of the effective charge in the 1:1 situation, it is however possible to obtain expressions that hold for all salinities.
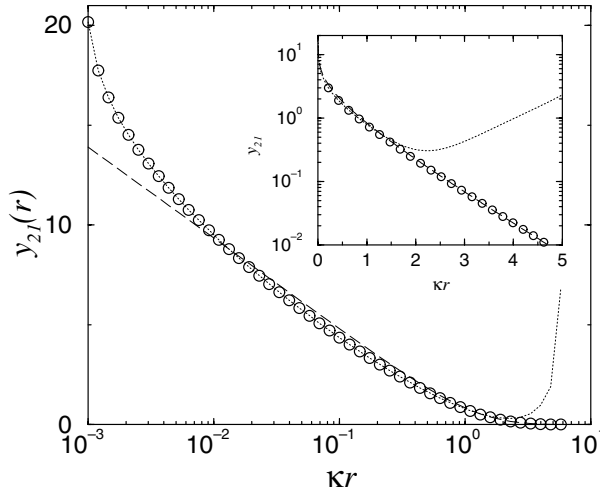
Figure 10. Electrostatic potential in a 2:1 electrolyte as a function of radial distance for a rod with a high bare charge ($\xi \simeq 11$) and $\kappa a = 10^{-3}$. The circles represent the numerical solution of PB theory, the dotted line is for the short distance formula (3.7c) and the dashed line is for the far field expression (1.3). In the inset, the same results are shown on a linear–log scale.
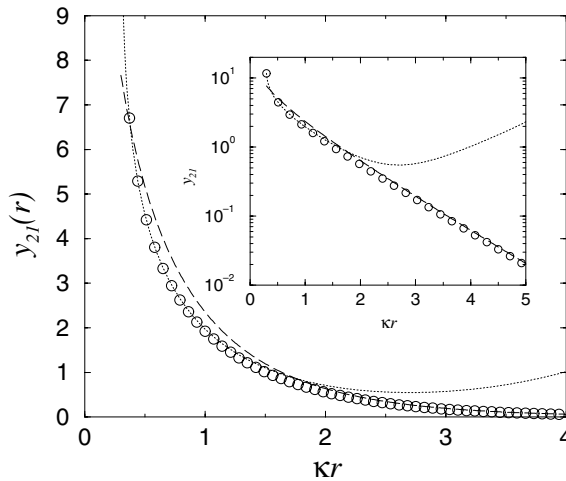

Figure 11. Same as figure 10 but with $\xi \simeq 40$ and $\kappa a = 0.3$, on a linear scale.

The effective charge at saturation, for any arbitrary value of $\tilde{a}$, has an interesting relation with the largest eigenvalue of the operators defined in equations (2.3) and (2.6). To see this, consider first the 1:1 electrolyte, and the solution (2.2) to the Poisson–Boltzmann equation. As the bare charge ξ increases the parameter λ (related to the effective charge ξ_{eff}) increases. At saturation ($\xi \to +\infty$), $\lambda = \lambda_{\text{sat}}$ is such that the electric field obtained from the solution (2.2) diverges at $\tilde{r} = \tilde{a}$. Clearly this happens if $\det(1 - \lambda K_{\tilde{a}}) = 0$, and thus if λ is the inverse of an eigenvalue of $K_{\tilde{a}}$.[7] Now, since when

---

[7] This analysis is for (positive) saturation when $\xi > 0$. In the case $\xi < 0$, the saturation is reached when $\det(1 + \lambda K_{\tilde{a}}) = 0$.
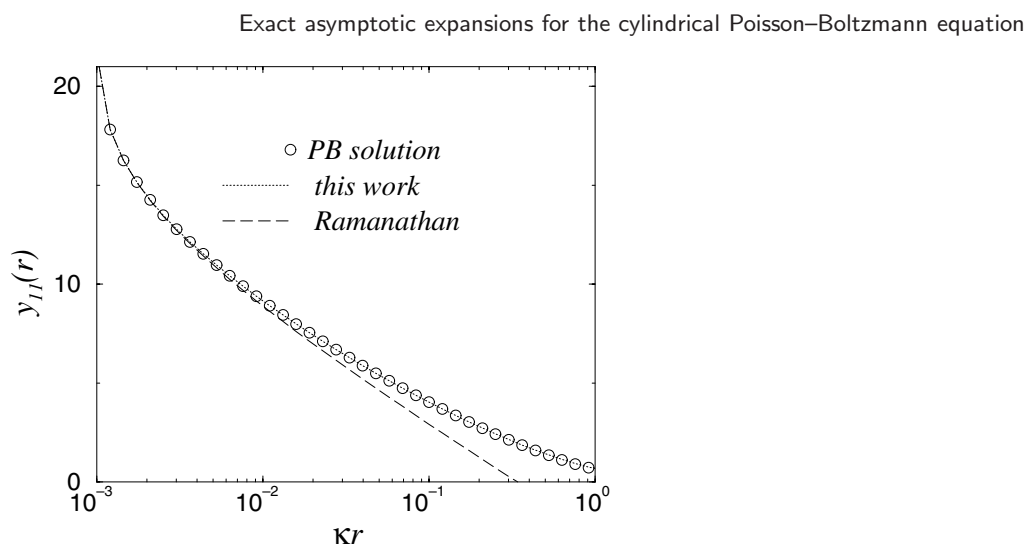
Figure 12. Comparison of the numerical solution of PB theory with expansion ($3.7a$) shown by the dotted line and with the formula of Ramanathan (see (5.1) and dashed line) for $\kappa a = 10^{-3}$, $\xi = 25$ and a 1:1 salt.
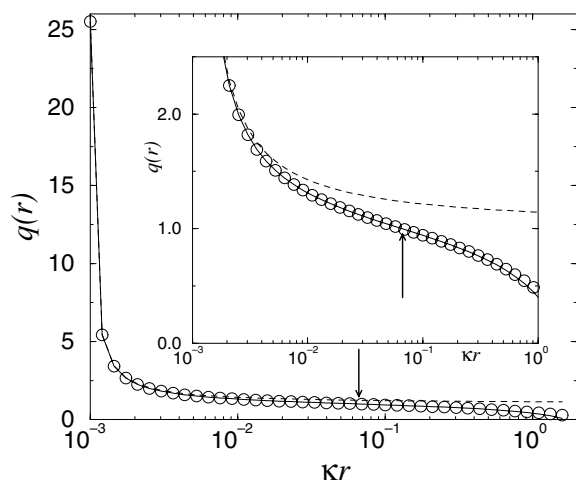

Figure 13. Integrated charge as a function of rescaled distance for the same parameters as in figure 12 (symbols and lines have the same meaning here). The inset shows the same data in the vicinity of the predicted Manning radius, indicated by the arrow. The prediction follows from ($5.6a$) or equivalently ($5.7a$) since we consider here a highly charged rod.

$\xi = 0$, $\lambda = 0$ and it increases as ξ increases, it appears that at saturation $\lambda = \lambda_{\mathrm{sat}}$ is equal to the inverse of the largest eigenvalue of $K_{\tilde{a}}$.

The same analysis applies to the 1:2 and 2:1 electrolytes. For a 1:2 electrolyte, for positive saturation $\xi \to +\infty$, λ_{sat} is the inverse of the largest eigenvalue of $K_{\tilde{a}}^{(2)}$, whereas for a 2:1 electrolyte, when $\xi \to +\infty$, λ_{sat} is the inverse of the largest eigenvalue of $-K_{\tilde{a}}^{(0)}$.

We have not been able to find explicitly the eigenvalues of the operators $K_{\tilde{a}}$, $K_{\tilde{a}}^{(0)}$ and $K_{\tilde{a}}^{(2)}$, for any arbitrary value of $\tilde{a}$. However one can use approximate methods to find estimates for the largest eigenvalue.

For the 1:1 electrolyte, it is shown in the appendix of [37] that for any function $\phi \in L^2(0, \infty, \mathrm{e}^{-\tilde{a}(u+u^{-1})/2}\,\mathrm{d}u)$, the largest eigenvalue $\lambda_{\mathrm{sat}}^{-1}$ of $K_{\tilde{a}}$ satisfies

$$\frac{(\phi, K_{\tilde{a}}\phi)}{(\phi, \phi)} \leq \lambda_{\mathrm{sat}}^{-1} \tag{6.1}$$

where $(\cdot, \cdot)$ is the scalar product of $L^2(0, \infty, \mathrm{e}^{-\tilde{a}(u+u^{-1})/2}\,\mathrm{d}u)$. Using the test function $\phi(u) = 1/\sqrt{u}$, we obtain

$$\lambda_{\mathrm{sat}} \leq \frac{K_0(\tilde{a})}{\pi\Gamma(0, 2\tilde{a})} \tag{6.2}$$

with K_0 the modified Bessel function and $\Gamma(0, z) = \int_z^{+\infty} \mathrm{e}^{-t}/t\,\mathrm{d}t$. Using equation (2.8a), this finally gives an upper bound for the effective charge at saturation, for a 1:1 electrolyte, for any arbitrary value of $\tilde{a}$, $\xi_{\mathrm{eff}}^{\mathrm{sat}} \leq \xi^{\mathrm{sat,up}}$, with

$$\xi^{\mathrm{sat,up}} = \frac{2aK_1(\tilde{a})K_0(\tilde{a})}{\pi\,\Gamma(0, 2\tilde{a})}. \tag{6.3}$$

As $\tilde{a} \to 0$, $\xi^{\mathrm{sat,up}} \to 2/\pi$, and thus has the same limit as the exact $\xi_{\mathrm{eff}}^{\mathrm{sat}}$. This is expected since in the appendix [37], this upper bound was used to prove that the supremum of the largest eigenvalue of $K_{\tilde{a}}$ as $\tilde{a} \to 0$ is π.

Interestingly, when $\tilde{a} \gg 1$ we have

$$\xi^{\mathrm{sat,up}} = 2\tilde{a} + \tfrac{3}{2} + \mathcal{O}(\tilde{a}^{-1}) \tag{6.4}$$

which is the same asymptotic behaviour as for the true effective saturated charge $\xi_{\mathrm{eff}}^{\mathrm{sat}}$ obtained in [38] by a and approach different to the present one. It is the effective charge of an infinite plane $(2\kappa a)$ plus a correction $(3/2)$ that is obtained using a small curvature expansion.

Figure 14 shows a comparison between $\xi^{\mathrm{sat,up}}$ from equation (6.3) and the effective charge at saturation $\xi_{\mathrm{eff}}^{\mathrm{sat}}$ obtained numerically. Surprisingly, it turns out $\xi^{\mathrm{sat,up}}$ is not only an upper bound for $\xi_{\mathrm{eff}}^{\mathrm{sat}}$ but also a very good estimate for $\xi_{\mathrm{eff}}^{\mathrm{sat}}$ for any value of $\tilde{a}$. If $\tilde{a} > 10^{-1}$ it is in very good agreement with the numerical data. However, for very small radius $\tilde{a} \ll 1$, the estimate (5.9a) of section 5.2, is better than the ansatz (6.3) (see the inset of figure 14 and compare it to figure 8).

7. Conclusion

The mathematical results derived in the framework of Painlevé/Toda type equations provide much insight into the screening behaviour of microions in the vicinity of a charged rod-like macroion. Although the mapping between the Poisson–Boltzmann equation for a certain class of electrolytes (1:1, 1:2 and 2:1) onto a Painlevé/Toda equation is in itself not new, previous analyses were concerned with the no salt limit where the ratio of macroion radius a to Debye length κ^{-1} vanishes, and the practical consequences and implications of a finite salt concentration had not been drawn. We have shown here that systematic logarithmic, and thus strong, corrections arise for various quantities of interest. All finite salt results reported here are new, and significantly improve previously available expressions. In addition, the 2:1 situation worked out here had not been considered before, even in the limit of vanishing salt content.
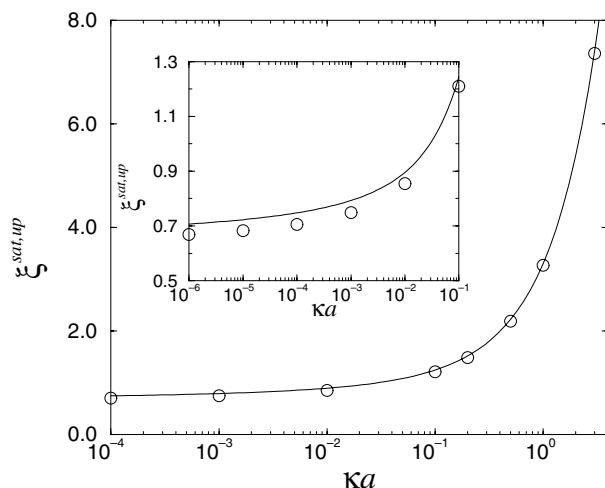
Figure 14. The upper bound (6.3) used as an ansatz for the effective charge at saturation as a function of the radius $\tilde{a}$ of the rod for a symmetric 1:1 electrolyte. The full line is the analytical expression (6.3), while the circles have been obtained by numerical resolution of Poisson–Boltzmann equation.

The experimental relevance of our findings has been sketched in the introduction. A rough criterion for the validity of our mean field approach is that $\Gamma = z^{3/2}\sqrt{\xi \ell_{\mathrm{B}}/(2\pi a)} < 2$ where z denotes the valency of counterions. For 1:1 and 2:1 electrolytes, the criterion is fulfilled even by the most highly charged polymers, such as double-stranded DNA for which $a \simeq 1$ nm and $\xi \simeq 4$, at least in water where $\ell_{\mathrm{B}} \simeq 0.7$ nm. In the 1:2 case, we obtain for dsDNA $\Gamma \simeq 2$, for which it is difficult to weight the importance of microionic correlation against the mean field effects reported here. In any case, our results apply to single-stranded DNA and polymers of lower line charge such as hyaluronan [39]. An upper limit should also be placed on the salt content ($\kappa \ell_{\mathrm{B}} < 1$), but such a requirement is irrelevant for our purposes since only the low salt regime has been discussed.

Section 3 contains the core of our analysis. It appeared there that the small scale behaviour of the electric potential depends on the position of the reduced bare charge ξ with respect to a threshold ξ_{c}. One may consider that this threshold is a remnant of its vanishing salt counterpart, which signals the onset of counterion condensation. It should be kept in mind however that counterion condensation is not an all or nothing process, but a gradually built up phenomenon.

The charge ξ_{c} is strongly salt dependent, and coincides with Manning critical value in the limit $\kappa a \to 0$. On the other hand, the large distance behaviour is always of the same functional form (see (1.3)) and is governed by the effective charge ξ_{eff}. This latter quantity depends on a parameter λ that also plays a crucial role in the description of the short distance behaviour. We have proposed a simple approximation for computing explicitly λ for 1:1, 2:1 and 1:2 electrolytes, from which all other quantities follow. The analytical predictions have been tested against the numerical solution of Poisson–Boltzmann theory, and shown to be remarkably accurate (of particular practical interest for highly charged polyelectrolytes are equations (3.7) and (1.3) with μ given by (4.13) and where λ is given as a function of μ in section 3.2). In particular, simple analytical results have been

derived for the Manning radius, that is often used to quantify the lateral extension of the condensate that may form around a cylindrical polyion. A few other measures of the condensate thickness have been commented upon.

Our approach is free of the matching procedures [40]–[42] or ad hoc though educated assumptions [43] underlying previous work, and therefore provides expansions with controlled error for the electric potential. The analysis of sections 3–5 requires that $a < \kappa^{-1}$. For larger salinities, contributions that have been neglected here become relevant. However, the spectral analysis of section 6 provides for all values of κa an upper bound for the far field signature of the polyion, from which an excellent approximation of the effective charge at saturation may be obtained.

The analytical results obtained emphasize the essential difference between the critical Manning charge for condensation and effective charge of the macroion, the latter being defined from the large scale electric behaviour. A consequence is that within a simplified two-state model where the population of microion is divided into a condensed region and a free population, free ions cannot be treated within a linearized theory, at variance with common belief and practice. Consistency with exact results requires that non-linear effects are still at work in the free region and significantly decrease the effective charge compared to the critical one. In the 1:2 case at ultralow salt, for all bare charges ξ larger than ξ_c, the ratio of ξ_{eff} to ξ_c (with ξ_c equal to ξ_{Manning} here since $\kappa a \to 0$) is equal to $\sqrt{3}/\pi \simeq 0.55$. This ratio is closer to unity for 2:1 electrolytes [$3\sqrt{3}/(2\pi) \simeq 0.83$], and intermediate for a 1:1 salt ($2/\pi \simeq 0.64$). We therefore emphasize that the distinction between bound and free ions is not only arbitrary but also potentially misleading.

Acknowledgments

Appendix A: Painlevé classification; a brief reminder

Polynomial non-linear differential equations of the form

$$A(x,y)\frac{\mathrm{d}^2 y}{\mathrm{d}x^2} + B(x,y)\frac{\mathrm{d}y}{\mathrm{d}x} + C(x,y)\left(\frac{\mathrm{d}y}{\mathrm{d}x}\right)^2 + D(x,y) = 0, \tag{A.1}$$

where the functions A, B, C, D are polynomial in y and analytic in x, have been classified with respect to the character of the singular points of the solutions. Of special interest are the equations for which branch points and essential singularities do not depend on initial conditions (and hence the only movable singularities are poles). Fifty canonical types of equations with the above property have been uncovered, most of which (44) are integrable in terms of elementary functions. Solving the remaining six types requires the introduction of new (Painlevé) transcendental functions. The third member (Painlevé III)

of this family of 6 corresponds to the generic form

$$xy\frac{\mathrm{d}^2 y}{\mathrm{d}x^2} = x\left(\frac{\mathrm{d}y}{\mathrm{d}x}\right)^2 - y\frac{\mathrm{d}y}{\mathrm{d}x} + ax + by + cy^3 + \mathrm{d}x\,y^4. \tag{A.2}$$

Appendix B: Short distance behaviour for $\lambda > \lambda_\mathrm{c}$

For a highly charged rod, when $\xi > \xi_\mathrm{c}$, we have $\mathrm{Re}(A) = \xi_\mathrm{Manning}$. Then, the last 'higher' order terms in equations (3.5) become of the same order as the $\mathcal{O}(1)$ terms. Thus the small $\tilde{r}$ asymptotics of $y(\tilde{r})$ are different, when $\xi > \xi_\mathrm{c}$, to the ones given by equations (3.5).

In [22] the asymptotics for $\lambda > 1$ in the 1:1 case were studied and in [24] the ones for the 1:2 case for $\lambda > \lambda_\mathrm{c}$ were obtained. We will not reproduce those calculations here, but to illustrate the method from [22, 24], we will compute the small $\tilde{r}$ asymptotics for the 2:1 case, for $\lambda > \lambda_\mathrm{c}^{(2:1)}$, which has not been previously considered.

The asymptotic form (3.5c) is actually valid even if λ is complex, provided that it satisfies (3.14). To study the asymptotics when $\lambda > \lambda_\mathrm{c}$ we can consider that λ approaches the cut $[\lambda_\mathrm{c}, +\infty)$ from below, for instance. Then we can rewrite (3.13b) as

$$A = 1 - \tfrac{3}{2}\mathrm{i}\mu \tag{B.1}$$

with

$$\mu = \frac{1}{\pi}\ln\left[\sqrt{\left(\frac{3\lambda}{2\lambda_\mathrm{c}} - \frac{1}{2}\right)^2 - 1} - \frac{1}{2} + \frac{3\lambda}{2\lambda_\mathrm{c}}\right] \tag{B.2a}$$

$$= \frac{1}{\pi}\cosh^{-1}\left(\frac{3\lambda}{2\lambda_\mathrm{c}} - \frac{1}{2}\right) > 0. \tag{B.2b}$$

Replacing into (3.5c) and keeping only the first two dominant terms (which are of the same order) gives

$$\mathrm{e}^{-y_{21}/2} = \frac{-\tilde{r}}{3\sqrt{6}\mu\mathrm{i}}\left(z - \bar{z}\right) + \mathcal{O}(\tilde{r}^8) \tag{B.3}$$

with

$$z = \left(\frac{\tilde{r}}{6\sqrt{3}}\right)^{3\mathrm{i}\mu/2}\left[\frac{\Gamma\left(1 - \mathrm{i}(\mu/2)\right)\Gamma(1 - \mathrm{i}\mu)}{\Gamma\left(1 + \mathrm{i}(\mu/2)\right)\Gamma(1 + \mathrm{i}\mu)}\right]^{1/2}. \tag{B.4}$$

If one chooses λ to approach the cut $[\lambda_\mathrm{c}, +\infty)$ from above then μ is changed into $-\mu$ and the final result is unchanged.

Finally, the potential y_{21} is given by

$$\mathrm{e}^{-y_{21}/2} = \frac{2\tilde{r}}{3\mu\sqrt{6}}\sin\left[-\frac{3\mu}{2}\ln\frac{\tilde{r}}{6\sqrt{3}} - \Psi^{(2:1)}(\mu)\right] + \mathcal{O}(\tilde{r}^8) \tag{B.5}$$

where

$$\Psi^{(2:1)}(\mu) = \mathrm{Im}\left\{\ln\left[\Gamma\left(1 - \frac{\mathrm{i}\mu}{2}\right)\Gamma(1 - \mathrm{i}\mu)\right]\right\}. \tag{B.6}$$

For the sake of completeness, we reproduce here small r asymptotics for the 1:1 and the 1:2 cases which were computed in [22] and [24], respectively. For the 1:1 electrolyte, when $\lambda > \lambda_{\mathrm{c}}^{(1:1)}$, the electric potential is given by

$$\mathrm{e}^{-y_{11}(\tilde{r})/2} = \frac{\tilde{r}}{4\mu} \sin\left[-2\mu \ln \frac{\tilde{r}}{8} + 2\Psi^{(1:1)}(\mu)\right] + \mathcal{O}(\tilde{r}^5) \qquad (\mathrm{B}.7a)$$

with

$$\mu = \frac{1}{\pi} \cosh^{-1}(\pi\lambda) > 0 \qquad (1:1) \qquad (\mathrm{B}.7b)$$

and

$$\Psi^{(1:1)}(\mu) = \mathrm{Im}\left[\ln \Gamma(1 + \mathrm{i}\mu)\right]. \qquad (\mathrm{B}.7c)$$

For the 1:2 electrolyte, when $\lambda > \lambda_{\mathrm{c}}^{(1:2)}$, the asymptotics are [24]

$$\mathrm{e}^{-y_{12}(\tilde{r})} = \frac{\tilde{r}}{3\mu\sqrt{3}} \sin\left[-3\mu \ln \frac{\tilde{r}}{6\sqrt{3}} - 2\Psi^{(1:2)}(\mu)\right] + \mathcal{O}(\tilde{r}^4) \qquad (1:2) \qquad (\mathrm{B}.8)$$

now with

$$\mu = \frac{1}{\pi} \cosh^{-1}\left(\frac{1}{2} + \frac{\lambda}{2\lambda_{\mathrm{c}}}\right) > 0 \qquad (\mathrm{B}.9)$$

and

$$\Psi^{(1:2)}(\mu) = \mathrm{Im}\left\{\ln\left[\Gamma\left(\frac{1-\mathrm{i}\mu}{2}\right)\Gamma(1-\mathrm{i}\mu)\right]\right\}. \qquad (\mathrm{B}.10)$$

For practical purposes, since μ is at most of order $1/|\ln \tilde{a}|$, we can expand the functions

$$\Psi^{(1:1)}(\mu) = -\gamma\mu + \mathcal{O}(\mu^3) \qquad (\mathrm{B}.11)$$

$$\Psi^{(1:2)}(\mu) = \mu\left(\tfrac{3}{2}\gamma + \ln 2\right) + \mathcal{O}(\mu^3) \qquad (\mathrm{B}.12)$$

$$\Psi^{(2:1)}(\mu) = 3\gamma\mu/2 + \mathcal{O}(\mu^3). \qquad (\mathrm{B}.13)$$

The asymptotics presented in equations (3.7) in the main text use this approximation for $\Psi(\mu)$.

In principle this means that our expressions in the main text for μ are accurate only to order $\mathcal{O}(1/|\ln \tilde{a}|^2)$. However, an explicit computation using further terms in the Taylor expansion of $\Psi(\mu)$ shows that our results, in the form presented in the main text, are actually accurate up to order $1/|\ln a|^3$ for μ and order $1/|\ln \tilde{a}|^4$ for the effective charges.

To illustrate this, consider, for example, the value of μ_{sat} for the 1:1 case. Using a Taylor expansion of $\Psi^{(1:1)}(\mu)$ up to order μ^3 gives

$$\mu_{\mathrm{sat}}^{(1:1)} = \frac{\pi}{2\ln(\tilde{a}/8)}\left[1 - \frac{\gamma}{\ln(\tilde{a}/8)} + \frac{\gamma^2}{(\ln(\tilde{a}/8))^2} - \frac{\gamma^3 + (\pi^2/24)\psi^{(2)}(1)}{(\ln(\tilde{a}/8))^3}\right] + \mathrm{O}\left((\ln \tilde{a})^{-5}\right) \,(\mathrm{B}.14)$$

where $\psi(x) = \mathrm{d}\ln \Gamma(x)/\mathrm{d}x$ is the digamma function and $\psi^{(2)}(x)$ its second derivative. Replacing this expression into equations (3.12) and (2.8), yields the effective charge at

saturation

$$\xi_{\text{sat}}^{(1:1)} = \tilde{a}K_1(\tilde{a})\left[\frac{2}{\pi} - \frac{\pi^3}{4\left(\ln(\tilde{a}/8)\right)^2} + \frac{\gamma\pi^3}{2\left(\ln(\tilde{a}/8)\right)^3} + \frac{-144\gamma^2\pi^3 + \pi^7}{192\left(\ln(\tilde{a}/8)\right)^4}\right.$$
$$\left. + \frac{\pi^3(48\gamma^3 - \gamma\pi^4 + \pi^2\psi^{(2)}(1))/48}{\left(\ln(\tilde{a}/8)\right)^5} + \mathrm{O}\left((\ln\tilde{a})^{-6}\right)\right]. \tag{B.15}$$

A direct comparison of equations (B.15) and (B.14) with (4.14a) and (5.9a) shows that the (more compact) expressions presented in the main text are indeed accurate up to order $1/|\ln a|^3$ for μ and order $1/|\ln\tilde{a}|^4$ for ξ_{sat}.

References

[1] Khokhlov A, 2000 *Soft and Fragile Matter* (*Scottish Graduate Textbook Series*) ed M E Cates and M R Evans (Bristol: IoP)
[2] Manning G S, 1969 *J. Chem. Phys.* **51** 924
[3] Oosawa F, 1971 *Polyelectrolytes* (New York: Dekker)
[4] Alfrey T Jr, Berg P W and Morawetz H, 1951 *J. Polym. Sci.* **7** 543
   Fuoss R M, Katchalsky A and Lifson S F, 1951 *Proc. Nat. Acad. Sci.* **37** 579
[5] Fixman M, 1979 *J. Chem. Phys.* **70** 4995
[6] Gueron M and Weisbuch G, 1980 *Biopolymers* **19** 353
[7] Ramanathan G V, 1983 *J. Chem. Phys.* **78** 3223
[8] Le Bret M and Zimm B H, 1984 *Biopolymers* **23** 287
[9] McCaskill J S and Fackerell E D, 1988 *J. Chem. Soc., Faraday Trans.* **84** 161
[10] Kholodenko A L and Beyerlein A L, 1995 *Phys. Rev. Lett.* **74** 4679
[11] Tracy C A and Widom H, 1997 *Physica* A **244** 402
[12] Levin Y, 1998 *Physica* A **257** 408
[13] Deserno M, Holm C and May S, 2000 *Macromolecules* **33** 199
[14] Hansen P L, Podgornik R and Parsegian V A, 2001 *Phys. Rev.* E **64** 021907
[15] O'Shaughnessy B and Yang Q, 2005 *Phys. Rev. Lett.* **94** 048302
[16] Belloni L, 2000 *J. Phys.: Condens. Matter* **12** R549
[17] Hansen J-P and Löwen H, 2000 *Ann. Rev. Phys. Chem.* **51** 209
[18] Grosberg A Y, Nguyen T T and Shklovskii B I, 2002 *Rev. Mod. Phys.* **74** 329
[19] Levin Y, 2002 *Rep. Prog. Phys.* **65** 1577
[20] Netz R R, 2001 *Eur. Phys. J.* E **5** 557
   Naji A and Netz R R, 2003 *Eur. Phys. J.* E **13** 43
[21] Levin Y, Trizac E and Bocquet L, 2003 *J. Phys.: Condens. Matter* **15** S3523
[22] McCoy B M, Tracy C A and Wu T T, 1977 *J. Math. Phys.* **18** 1058
[23] Widom H, 1997 *Commun. Math. Phys.* **184** 653
[24] Tracy C A and Widom H, 1998 *Commun. Math. Phys.* **190** 697
[25] Trizac E and Téllez G, 2006 *Phys. Rev. Lett.* **96** 038302
[26] See e.g. Davis H T, 1962 *Introduction to Nonlinear Differential and Integral Equations* (New York: Dover)
[27] Benham C J, 1983 *J. Chem. Phys.* **79** 1969
[28] Šamaj L and Travěnec I, 2000 *J. Stat. Phys.* **101** 713
[29] Cornu F and Jancovici B, 1987 *J. Stat. Phys.* **49** 33
[30] Odijk T, 1983 *Chem. Phys. Lett.* **100** 145
[31] Trizac E, Bocquet L, Aubouy M and von Grünberg H H, 2003 *Langmuir* **19** 4027
[32] Téllez G and Trizac E, 2004 *Phys. Rev.* E **70** 011404
[33] Téllez G and Trizac E, 2003 *Phys. Rev.* E **68** 061401
[34] Netz R R and Joanny J-F, 1998 *Macromolecules* **31** 5123
[35] Weisbuch G and Gueron M, 1981 *J. Phys. Chem.* **85** 517
[36] Qian H and Schellman J A, 2000 *J. Phys. Chem.* B **104** 11528
[37] Tracy C A, 1991 *Commun. Math. Phys.* **142** 297
[38] Aubouy M, Trizac E and Bocquet L, 2003 *J. Phys. A: Math. Gen.* **36** 5835
[39] Buhler E and Boué F, 2004 *Macromolecules* **37** 1600
[40] MacGillivray A D and Winkleman J J Jr, 1965 *J. Chem. Phys.* **45** 2184
[41] Philip J R and Wooding R A, 1970 *J. Chem. Phys.* **52** 953
[42] van Keulen H and Smit J A M, 1995 *J. Colloid Interface Sci.* **170** 134
[43] Tuinier R, 2003 *J. Colloid Interface Sci.* **258** 45